ACADEMIC PRESS

Available online at www.sciencedirect.com

SCIENCE DIRECT®

Journal of Sound and Vibration 262 (2003) 419–455

JOURNAL OF SOUND AND VIBRATION

www.elsevier.com/locate/jsvi

Examination of multi-dimensional vibration isolation measures and their correlation to sound radiation over a broad frequency range

Rajendra Singh*, Seungbo Kim

Acoustics and Dynamics Laboratory, Department of Mechanical Engineering and The Center for Automotive Research, The Ohio State University, Columbus, OH 43210-1107, USA

Received 13 November 2001; accepted 9 July 2002

Abstract

This article examines alternate vibration isolation measures for a multi-dimensional system. The isolator and receiver are modelled by the continuous system theory. The source is assumed to be rigid and both force and moment excitations are considered. Our analysis is limited to a linear time-invariant system, and the mobility synthesis method is adopted to describe the overall system behavior. Inverted 'L' beam and plate receivers are employed here to incorporate the contribution of their in-plane motions to vibration powers and radiated sound. Multi-dimensional transmissibilities and effectivenesses are comparatively evaluated along with power-based measures for the inverted 'L' beam receiver and selected source configurations. Further, sound pressures radiated from the inverted 'L' beam receiver are calculated and correlated with power transmitted to the receiver. Interactions within the 'L' beam receiver are also analyzed and measures that could identify dominant transfer paths within a system are examined. Sound measurements and predictions for the inverted 'L' plate receiver demonstrate that a rank order based on free field sound pressures, at one or more locations, may be regarded as a measure of isolation performance. Measured insertion losses for sound pressure match well with those based on computed results although further study is needed in relation to some discrepancies shown in the results. Finally, several emerging research topics are identified.

*Corresponding author. Tel.: +1-614-292-9044; fax: +1-614-292-3163.
E-mail address: singh.3@osu.edu (R. Singh).

0022-460X/03/$ - see front matter
doi:10.1016/S0022-460X(03)00105-6

1. Introduction

Force or velocity transmissibility and related concepts are widely used, mostly for uni-directional motions [1–5] but have been extended to multi-dimensional systems [6]. Also, the force or velocity effectiveness term, the ratio of transmitted force or velocity with an isolator to the one without the isolator, has been employed for both uni-directional [1,2,4] and multi-dimensional problems [7,8]. However, for a multi-dimensional problem, the units of translational and rotational quantities are not compatible [9–11]. For this reason, the concept of vibration power has been used to assess transmission to receivers [11–16]. Application of such measures includes structural discontinuities [17,18], vibration isolators [11–16], and bearings [19]. The transmission efficiency, the ratio of input vibration power to transmitted power, has been studied for propagating waves at the interface of infinite structures [17,18]. Input and transmitted powers have also been compared for some finite structures [15,20,21].

For a multi-dimensional system, strong interactions occur between the coupled degrees of freedom. For example, Cremer and Heckle [17] claim that the moment mobility must be dealt with via a matrix in the presence of flexural motions. They have also explained that the coupling mobility in flexural motions may suppress the bending waves under some conditions. This concept has been implemented to attenuate vibration input to a single structure [9]. Further, some separation of transfer paths has been experimentally investigated [22]. Nonetheless, a proper quantification or interpretation of dynamic interactions that occur among coupled structural paths has not been addressed. Furthermore, the quantification of structure-borne energy and source strengths still remain as key obstacles in many cases [23–27]. Satisfactory resolution of such research issues would require appropriate vibration transmission measures. However, such measures for a multi-dimensional system are not well understood and often left to the discretion of user [1,7,28]. In this article, we address this particular issue with emphasis on a multi-dimensional isolator (of distributed parameters) in the presence of a compliant receiver.

2. Problem formulation

The problem is defined via Figs. 1 and 2, in the context of source, path (isolator) and receiver. The scope of this study is limited to the analysis of a linear time-invariant (LTI) system with a single isolator (defined in terms of distributed parameter). In this multi-dimensional system, the source is described by a rigid body and two alternate compliant receivers, namely the inverted 'L' beam and plate structures, are utilized for analytical and experimental studies. Harmonic force and moment excitations are applied to the source, up to 2.5 kHz. Mobilities of each component are analytically or computationally obtained, and then the mobility synthesis method is employed to predict the harmonic response of the overall system, based on the formulation reported in our earlier article [29]. Source characteristics that have been previously investigated are also utilized here [12]. Chief objectives of this study include: (1) Examine alternate measures of vibration isolation performance for a multi-dimensional system and quantify the vibration transmission for several system configurations. (2) Calculate and measure the sound generated from the 'L' structure receiver and correlate results with vibration isolation measures. Key concepts will be illustrated via experimental and analytical studies on selected isolators.

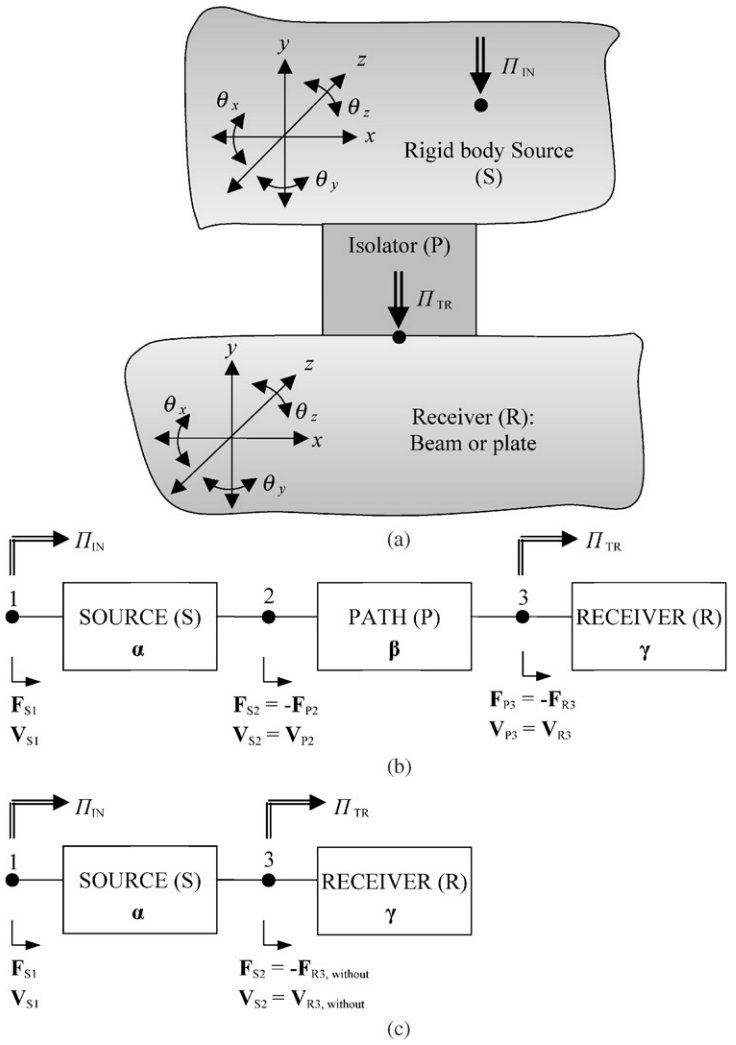

Fig. 1. Problem formulation for vibration transmission: (a) multi-dimensional path isolator; (b) source–path–receiver system and their mobility matrices $\boldsymbol{\alpha}$, $\boldsymbol{\beta}$ and $\boldsymbol{\gamma}$; (c) vibration system without isolator. Here, $\mathbf{F}$ and $\mathbf{V}$ are vectors.

3. Vibration isolation measures

3.1. Multi-dimensional formulation

Interfacial forces ($\mathbf{F}$) in Fig. 1 are as follows when an external force vector is applied at location 1. Note that $\boldsymbol{\alpha}_{ij}$, $\boldsymbol{\beta}_{ij}$ and $\boldsymbol{\gamma}_{ij}$ represent the mobility matrices of source, path and receiver, respectively; a detailed analysis has been reported in an earlier paper by the same authors [29]. Here, all formulations are in the frequency domain though the ubiquitous (ω) term has been dropped for the sake of brevity:

$$\mathbf{F}_{P2} = [[\boldsymbol{\alpha}_{22} + \boldsymbol{\beta}_{22}] - \boldsymbol{\beta}_{23}[\boldsymbol{\beta}_{33} + \boldsymbol{\gamma}_{33}]^{-1}\boldsymbol{\beta}_{32}]^{-1}\boldsymbol{\alpha}_{21}\mathbf{F}_{S1}, \tag{1a}$$

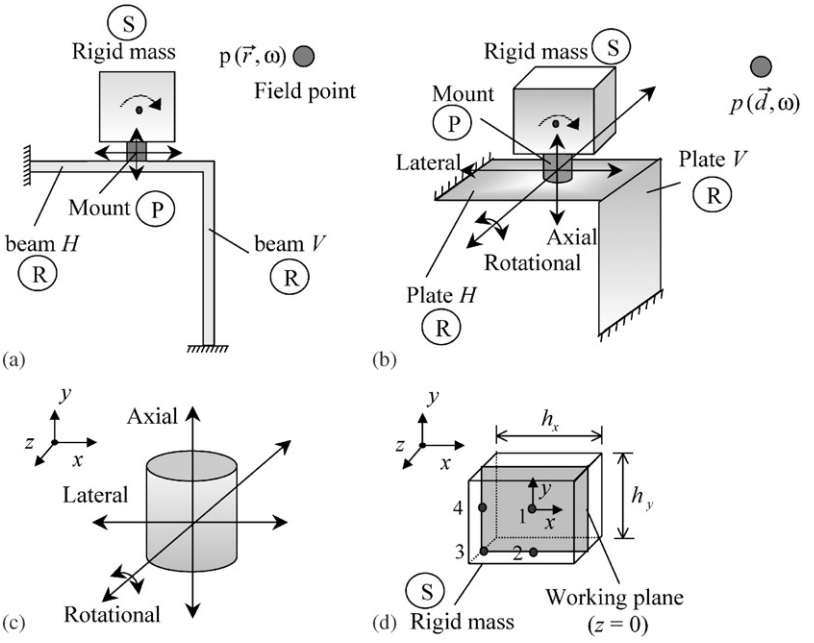

Fig. 2. Configuration of the analytical vibration isolation system: (a) system with an inverted 'L' beam receiver; (b) system with an inverted 'L' plate receiver; (c) a cylindrical isolator with vibration transmission components; (d) isolator location $[x, y, z]$ on the working plane of a cubic rigid body source: case $1 = [0, 0, 0]$; case $2 = [0, -h_y/2, 0]$; case $3 = [-h_x/2, -h_y/2, 0]$; case $4 = [-h_x/2, 0, 0]$.

$$\mathbf{F}_{R3} = [[\boldsymbol{\beta}_{33} + \boldsymbol{\gamma}_{33}] - \boldsymbol{\beta}_{32}[\boldsymbol{\alpha}_{22} + \boldsymbol{\beta}_{22}]^{-1}\boldsymbol{\beta}_{23}]^{-1}\boldsymbol{\beta}_{32}[\boldsymbol{\alpha}_{22} + \boldsymbol{\beta}_{22}]^{-1}\boldsymbol{\alpha}_{21}\mathbf{F}_{S1}. \tag{1b}$$

Also, velocities ($\mathbf{V}$) at intermediate locations when an external force is applied at 1 are as follows where $\mathbf{M}$ is the system mobility matrix:

$$\mathbf{V}_1 = \mathbf{M}_{11}\mathbf{F}_{S1} = [\boldsymbol{\alpha}_{11} + \boldsymbol{\alpha}_{12}[\boldsymbol{\beta}_{23}[\boldsymbol{\beta}_{33} + \boldsymbol{\gamma}_{33}]^{-1}\boldsymbol{\beta}_{32} - [\boldsymbol{\alpha}_{22} + \boldsymbol{\beta}_{22}]]^{-1}\boldsymbol{\alpha}_{21}]\mathbf{F}_{S1}, \tag{2a}$$

$$\mathbf{V}_2 = \mathbf{M}_{21}\mathbf{F}_{S1} = [\boldsymbol{\alpha}_{21} - \boldsymbol{\alpha}_{22}[[\boldsymbol{\alpha}_{22} + \boldsymbol{\beta}_{22}] - \boldsymbol{\beta}_{23}[\boldsymbol{\beta}_{33} + \boldsymbol{\gamma}_{33}]^{-1}\boldsymbol{\beta}_{32}]^{-1}\boldsymbol{\alpha}_{21}]\mathbf{F}_{S1}, \tag{2b}$$

$$\mathbf{V}_3 = \mathbf{M}_{31}\mathbf{F}_{S1} = \boldsymbol{\gamma}_{33}[[\boldsymbol{\beta}_{33} + \boldsymbol{\gamma}_{33}] - \boldsymbol{\beta}_{32}[\boldsymbol{\alpha}_{22} + \boldsymbol{\beta}_{22}]^{-1}\boldsymbol{\beta}_{23}]^{-1}\boldsymbol{\beta}_{32}[\boldsymbol{\alpha}_{22} + \boldsymbol{\beta}_{22}]^{-1}\boldsymbol{\alpha}_{21}\mathbf{F}_{S1}. \tag{2c}$$

3.2. Force and velocity transmissibility matrices

The multi-dimensional force transmissibility matrix ($\mathbf{TR}_F$) can be defined from Eq. (1b) and likewise the velocity transmissibility matrix ($\mathbf{TR}_V$) can be developed using Eqs. (2a) and (2c) as follows where/represents a quotient operation for matrices:

$$\mathbf{TR}_F = \mathbf{F}_{R3}/\mathbf{F}_{S3} = [[\boldsymbol{\beta}_{33} + \boldsymbol{\gamma}_{33}] - \boldsymbol{\beta}_{32}[\boldsymbol{\alpha}_{22} + \boldsymbol{\beta}_{22}]^{-1}\boldsymbol{\beta}_{23}]^{-1}\boldsymbol{\beta}_{32}[\boldsymbol{\alpha}_{22} + \boldsymbol{\beta}_{22}]^{-1}\boldsymbol{\alpha}_{21}, \tag{3a}$$

$$\mathbf{TR}_V = \mathbf{V}_{R3}/\mathbf{V}_{S3} = \mathbf{M}_{31}\mathbf{M}_{11}^{-1}. \tag{3b}$$

For uni-directional motions, the transmissibility (TR) is a non-dimensional scalar quantity, and therefore the diagonal terms of $\mathbf{TR}$ are non-dimensional. But, the units of off-diagonal terms vary since each off-diagonal component represents a specific coupling between related forces and motions. Further, the modified force transmissibility matrix ($\mathbf{TR}_F^b$) can be defined as follows by using Eq. (1b) for F_{R3} and substituting the null matrix for $\boldsymbol{\beta}$ and $\boldsymbol{\gamma}$ into Eq. (1a) for $\mathbf{F}_{P2}^b$; here the superscript b represents the blocked force [2]:

$$\mathbf{TR}_F^b = \mathbf{F}_{R3}/\mathbf{F}_{P2}^b = [[\boldsymbol{\beta}_{33} + \boldsymbol{\gamma}_{33}] - \boldsymbol{\beta}_{32}[\boldsymbol{\alpha}_{22} + \boldsymbol{\beta}_{22}]^{-1}\boldsymbol{\beta}_{23}]^{-1}\boldsymbol{\beta}_{32}[\boldsymbol{\alpha}_{22} + \boldsymbol{\beta}_{22}]^{-1}\boldsymbol{\alpha}_{22}. \tag{4}$$

Similarly, the modified velocity transmissibility matrix ($\mathbf{TR}_V^f$) can also be introduced as follows by using Eq. (2c) and noticing $\mathbf{V}_{S2}^f = \boldsymbol{\alpha}_{21}\mathbf{F}_{S1}$; here the superscript f denotes free velocity at the source output [2]:

$$\mathbf{TR}_V^f = \mathbf{V}_{R3}/\mathbf{V}_{S2}^f = \boldsymbol{\gamma}_{33}[[\boldsymbol{\beta}_{33} + \boldsymbol{\gamma}_{33}] - \boldsymbol{\beta}_{32}[\boldsymbol{\alpha}_{22} + \boldsymbol{\beta}_{22}]^{-1}\boldsymbol{\beta}_{23}]^{-1}\boldsymbol{\beta}_{32}[\boldsymbol{\alpha}_{22} + \boldsymbol{\beta}_{22}]^{-1}. \tag{5}$$

Again, the units of off-diagonal terms in modified transmissibility matrices vary even though the diagonal terms are non-dimensional.

3.3. Force and velocity effectiveness matrices

Multi-dimensional representation of the effectiveness concept can be extended to isolators that are described by uncoupled spring elements [7]. To illustrate this measure, consider the interfacial force and response at location 3 for a system without any isolator. These can be obtained by synthesizing only the source and receiver ($\boldsymbol{\alpha}$ and $\boldsymbol{\gamma}$); details may be found in literature [29]:

$$\mathbf{F}_{R3,without} = [\boldsymbol{\alpha}_{22} + \boldsymbol{\gamma}_{33}]^{-1}\boldsymbol{\alpha}_{21}\mathbf{F}_{S1}, \quad \mathbf{V}_{R3,without} = \boldsymbol{\gamma}_{33}[\boldsymbol{\alpha}_{22} + \boldsymbol{\gamma}_{33}]^{-1}\boldsymbol{\alpha}_{21}\mathbf{F}_{S1}. \tag{6a, b}$$

The force effectiveness matrix $\boldsymbol{\Xi}_\mathbf{F}$ is obtained by using Eqs. (1b) and (6a) for the with and without isolator cases, respectively:

$$\begin{aligned}\boldsymbol{\Xi}_\mathbf{F} &= \mathbf{F}_{3,with}/\mathbf{F}_{3,without} \\ &= [[\boldsymbol{\beta}_{33} + \boldsymbol{\gamma}_{33}] - \boldsymbol{\beta}_{32}[\boldsymbol{\alpha}_{22} + \boldsymbol{\beta}_{22}]^{-1}\boldsymbol{\beta}_{23}]^{-1}\boldsymbol{\beta}_{32}[\boldsymbol{\alpha}_{22} + \boldsymbol{\beta}_{22}]^{-1}[\boldsymbol{\alpha}_{22} + \boldsymbol{\gamma}_{33}].\end{aligned} \tag{7}$$

Further, relating Eq. (1c) to Eq. (6b) leads to the velocity effectiveness matrix $\boldsymbol{\Xi}_\mathbf{V}$:

$$\begin{aligned}\boldsymbol{\Xi}_\mathbf{V} &= \mathbf{V}_{3,with}/\mathbf{V}_{3,without} \\ &= \boldsymbol{\gamma}_{33}[[\boldsymbol{\beta}_{33} + \boldsymbol{\gamma}_{33}] - \boldsymbol{\beta}_{32}[\boldsymbol{\alpha}_{22} + \boldsymbol{\beta}_{22}]^{-1}\boldsymbol{\beta}_{23}]^{-1}\boldsymbol{\beta}_{32}[\boldsymbol{\alpha}_{22} + \boldsymbol{\beta}_{22}]^{-1}[\boldsymbol{\alpha}_{22} + \boldsymbol{\gamma}_{33}]\boldsymbol{\gamma}_{33}^{-1}.\end{aligned} \tag{8}$$

3.4. Vibration power

The time-averaged vibrational power input Π_{IN} to a structure for a uni-directional motion is defined as follows, given a point harmonic excitation $F\mathrm{e}^{\mathrm{i}\omega t}$ and the resultant velocity $V\mathrm{e}^{\mathrm{i}\omega t}$ at the driving point where F and V are complex-valued amplitudes:

$$\begin{aligned}\Pi_{IN}(\omega) &= \frac{\omega}{2\pi}\int_0^{2\pi/\omega} F(t)V(t)\,\mathrm{d}t = \tfrac{1}{2}|F|\,|V|\cos\phi \\ &= \tfrac{1}{2}\,\mathrm{Re}[\tilde{F}(\omega)\tilde{V}^*(\omega)] = \tfrac{1}{2}\,\mathrm{Re}[\tilde{V}(\omega)\tilde{F}^*(\omega)].\end{aligned} \tag{9}$$

Here, Re and superscript * denote the real value and the conjugate of a complex quantity, respectively. Similarly, the harmonic power Π at any location is as follows, given harmonic excitation $\mathbf{F}e^{i\omega t}$ and response velocity $\mathbf{V}e^{i\omega t}$ vectors where the superscript T denotes the transpose of a vector:

$$\Pi(\omega) = \tfrac{1}{2}\,\mathrm{Re}[\mathbf{F}^{\mathrm{T}}(\omega)\mathbf{V}^{*}(\omega)] = \tfrac{1}{2}\,\mathrm{Re}[\mathbf{V}^{\mathrm{T}}(\omega)\mathbf{F}^{*}(\omega)]. \tag{10}$$

Power transmitted by each path (i) at a connection of interest is related to the mobility matrix (M) of that component by

$$\Pi_i = \tfrac{1}{2}\,\mathrm{Re}[F_i V_i^{*}] = \frac{1}{2}\sum_j \mathrm{Re}[F_i F_j^{*} M_{ij}^{*}], \tag{11}$$

where F_i and F_j are the ith and the jth components of excitation at the junction and M_{ij} represents the ij mobility component which relates the ith velocity and the jth force where M is the driving point mobility matrix of subsequent structure. For the sake of illustration, consider a planer motion that is represented by $\mathbf{F} = [f_x\ \ f_y\ \ q_z]^{\mathrm{T}}e^{i\omega t}$ and $\mathbf{V} = [v_x\ \ v_y\ \ w_z]^{\mathrm{T}}e^{i\omega t}$. Total power ($\Pi_{Total}$) transmitted to the structure by force (f_x,f_y) and moment (q_z) components is

$$\begin{aligned}\Pi_{Total} = {} & \tfrac{1}{2}|f_x|^2\ \mathrm{Re}[M_{xx}] + \tfrac{1}{2}\,\mathrm{Re}[f_x f_y^{*} M_{xy}^{*}] + \tfrac{1}{2}\,\mathrm{Re}[f_x q_z^{*} M_{xz}^{*}] \\ & + \tfrac{1}{2}\,\mathrm{Re}[f_y f_x^{*} M_{yx}^{*}] + \tfrac{1}{2}|f_y|^2\ \mathrm{Re}[M_{yy}] + \tfrac{1}{2}\,\mathrm{Re}[f_y q_z^{*} M_{yz}^{*}] \\ & + \tfrac{1}{2}\,\mathrm{Re}[q_z f_x^{*} M_{zx}^{*}] + \tfrac{1}{2}\,\mathrm{Re}[q_z f_y^{*} M_{zy}^{*}] + \tfrac{1}{2}|q_z|^2\ \mathrm{Re}[M_{zz}].\end{aligned} \tag{12}$$

Therefore, the input (IN) power at driving point (k) and the transmitted (TR) power at connection point (l) are, respectively,

$$\Pi_{IN} = \tfrac{1}{2}\,\mathrm{Re}[\mathbf{F}_{IN}^{\mathrm{T}}\mathbf{V}_k^{*}] = \tfrac{1}{2}\,\mathrm{Re}[\mathbf{F}_{IN}^{\mathrm{T}}[\mathbf{M}_{kk}\mathbf{F}_{IN}]^{*}], \tag{13a}$$

$$\Pi_{TR} = \tfrac{1}{2}\,\mathrm{Re}[\mathbf{F}_{TR}^{\mathrm{T}}\mathbf{V}_l^{*}] = \tfrac{1}{2}\,\mathrm{Re}[\mathbf{F}_{TR}^{\mathrm{T}}[\mathbf{M}_{lk}\mathbf{F}_{IN}]^{*}] = \tfrac{1}{2}\,\mathrm{Re}[\mathbf{F}_{TR}^{\mathrm{T}}[\mathbf{M}_{ll}\mathbf{F}_{TR}]^{*}], \tag{13b}$$

where $\mathbf{M}_{kk}$ and $\mathbf{M}_{lk}$ are the mobility matrices of the combined structure, and $\mathbf{M}_{ll}$ is the driving point mobility matrix of the subsequent structure only. Since several coupling mobility terms between forces and moments exist, each component of the transmitted power may be positive or negative. However, the power components that are related to the diagonal terms in the driving point mobility of a receiver are always positive since the real part of the diagonal terms in the driving point mobility and the mean-square transmitted force are always positive. Note that the power component for each degree of freedom is interrelated to other power components since the coupled terms in Eq. (12) are associated with two motion or excitation variables in different degrees of freedom. In our study, the sum of power components that are related to coupling mobility of a receiver, as given by Eq. (12), is defined as the coupling power and such coupling powers may be positive or negative.

3.5. Mean-square force and velocity Ψ_W^2

The mean-square force Ψ_F^2 and velocity Ψ_V^2 at the interface (location 3 in Fig. 1) between isolator and receiver for uni-directional motions are, respectively:

$$\Psi_F^2 = \langle F_3^2(t)\rangle_t = \frac{\omega}{2\pi}\int_0^{2\pi/\omega} F_3^2(t)\,\mathrm{d}t = \tfrac{1}{2}\,\mathrm{Re}[\tilde{F}_3\tilde{F}_3^{*}] = \frac{|F_3|^2}{2}, \tag{14a}$$

$$\Psi_V^2 = \langle V_3^2(t) \rangle_t = \frac{\omega}{2\pi} \int_0^{2\pi/\omega} V_3^2(t)\, \mathrm{d}t = \tfrac{1}{2}\,\mathrm{Re}[\tilde{V}_3 \tilde{V}_3^*] = \frac{|V_3|^2}{2}. \tag{14b}$$

Here, $\langle\ \rangle_t$ and $||$ represent time-averaged and absolute values respectively. The Ψ_F^2 and Ψ_V^2 terms are meaningful for uni-directional motions but their relative comparisons are inappropriate for multi-dimensional motions since the units of Ψ^2 terms are not compatible between translational and rotational directions. For instance, it is not suitable to compare the mean-square force (N^2) and the mean-square moment ($N^2\,m^2$). For this reason, the concept of a weighted mean-square quantity Ψ_W^2 that can hold equivalent units for dissimilar variables is proposed via Eq. (15). By employing Ψ_W^2, a rank ordering of transfer paths is feasible for multi-dimensional motions. In this study, we choose the driving point mobility M (or its reciprocal that is impedance Z), corresponding to the force (or velocity) variable, as a weighting factor. By adopting the M or Z of receiver at location 3, define the Ψ_{WF}^2 and Ψ_{WV}^2 for uni-directional motions as

$$\Psi_{WF}^2 = \tfrac{1}{2}\,\mathrm{Re}[\tilde{F}_3 \tilde{F}_3^* M_{33}] = \frac{|F_3|^2}{2}\,\mathrm{Re}[M_{33}], \qquad \Psi_{WV}^2 = \tfrac{1}{2}\,\mathrm{Re}[\tilde{V}_3 \tilde{V}_3^* Z_{33}] = \frac{|V_3|^2}{2}\,\mathrm{Re}[Z_{33}]. \tag{15a, b}$$

The Ψ_{WF}^2 and Ψ_{WV}^2 have the units of power and are always positive since the real parts of driving point mobility and impedance are positive. Further, the Ψ_{WF}^2 (or Ψ_{WV}^2) represents the power term consisting of force (or moment) and corresponding velocity. The total weighted mean-square force $\Psi_{WF,Total}^2$ and velocity $\Psi_{WV,Total}^2$ can be defined at multi-dimensional interfacial location (3) in Fig. 1 as

$$\Psi_{WF,Total}^2 = \tfrac{1}{2}\,\mathrm{Re}[\tilde{\mathbf{F}}_3^{\mathrm{T}}\ \mathrm{diag}[\mathbf{M}_{33}]\tilde{\mathbf{F}}_3^*], \qquad \Psi_{WV,Total}^2 = \tfrac{1}{2}\,\mathrm{Re}[\tilde{\mathbf{V}}_3^{\mathrm{T}}\ \mathrm{diag}[\mathbf{Z}_{33}]\tilde{\mathbf{V}}_3^*]. \tag{16a, b}$$

For a planer motion example that was presented in the previous section, the $\Psi_{WF,Total}^2$ and $\Psi_{WV,Total}^2$ are expanded as

$$\Psi_{WF,Total}^2 = \tfrac{1}{2}|f_x|^2\ \mathrm{Re}[M_{xx}] + \tfrac{1}{2}|f_y|^2\ \mathrm{Re}[M_{yy}] + \tfrac{1}{2}|q_z|^2\ \mathrm{Re}[M_{zz}], \tag{17a}$$

$$\Psi_{WV,Total}^2 = \tfrac{1}{2}|v_x|^2\ \mathrm{Re}[Z_{xx}] + \tfrac{1}{2}|v_y|^2\ \mathrm{Re}[Z_{yy}] + \tfrac{1}{2}|w_z|^2\ \mathrm{Re}[Z_{zz}]. \tag{17b}$$

Therefore, $\Psi_{WF,Total}^2$ is the sum of power components that are related to the driving point mobilities of the receiver, and $\Psi_{WV,Total}^2$ is the sum of power components that are related to the driving point impedances of the receiver. Also, the individual mean-square force and velocity terms are scalar quantities.

3.6. Structure-borne or airborne noise measures

For two adjacent infinite structures, the transmission efficiency Γ (a non-dimensional scalar quantity) has been defined as the ratio of transmitted power Π_{TR} to incident power Π_{IN} [17,18]. For a finite structure, Γ can be defined in the same fashion as

$$\Gamma = \frac{\Pi_{TR}}{\Pi_{IN}}. \tag{18}$$

The effectiveness Ξ_Π of vibration power (a non-dimensional scalar quantity) can be defined as follows where "with" implies the net power transmitted to receiver with an isolator and "without"

Table 1
Summary of frequency-domain vibration isolation measures for multi-dimensional motions

Measure	Definition as a function of ω
Force and motion transmissibilities [6,8]	$\mathbf{TR}_F = \mathbf{F}_{R3}/\mathbf{F}_{S1}$ and $\mathbf{TR}_V = \mathbf{V}_{R3}/\mathbf{V}_{S1}$
Modified force and motion transmissibilities	$\mathbf{TR}_F^b = \mathbf{F}_{R3}/\mathbf{F}_{P2}^b$ and $\mathbf{TR}_V^f = \mathbf{V}_{R3}/\mathbf{V}_{S2}^f$
Force and motion effectivenesses [7]	$\mathbf{\Xi}_\mathbf{V} = \mathbf{V}_{3,with}/\mathbf{V}_{3,without}$ and $\mathbf{\Xi}_\mathbf{F} = \mathbf{F}_{3,with}/\mathbf{F}_{3,without}$
Mean-square force and velocities at receiver input	$\Psi_F^2 = \langle F_3^2(t)\rangle_t = \frac{1}{2}\,\mathrm{Re}[\tilde{F}_3\tilde{F}_3^*] = \frac{\lvert F_3\rvert^2}{2}$ and $\Psi_V^2 = \langle V_3^2(t)\rangle_t = \frac{1}{2}\,\mathrm{Re}[\tilde{V}_3\tilde{V}_3^*] = \frac{\lvert V_3\rvert^2}{2}$
Weighted mean-square force and velocities at receiver input	$\Psi_{WF,Total}^2 = \frac{1}{2}\,\mathrm{Re}[\tilde{\mathbf{F}}_3^{\mathrm{T}}\ \mathrm{diag}[\mathbf{M}_{33}]\tilde{\mathbf{F}}_3^*]$ and $\Psi_{WV,Total}^2 = \frac{1}{2}\,\mathrm{Re}[\tilde{\mathbf{V}}_3^{\mathrm{T}}\ \mathrm{diag}[\mathbf{Z}_{33}]\tilde{\mathbf{V}}_3^*]$
Power transmitted to receiver input [9–16,19–21]	$\Pi_{TR}(\omega) = \frac{1}{2}\,\mathrm{Re}[\mathbf{F}^{\mathrm{T}}\mathbf{V}^*] = \frac{1}{2}\,\mathrm{Re}[\mathbf{V}^{\mathrm{T}}\mathbf{F}^*]$
Efficiency of vibration power transmitted to receiver input [15,20,21]	$\Gamma(\omega) = \frac{\Pi_{TR}}{\Pi_{IN}}$
Effectiveness of vibration power transmitted to receiver input [20,21]	$\Xi_\Pi(\omega) = \frac{\Pi_{TR,with}}{\Pi_{TR,without}}$
Vibration or sound amplitudes at the receiver	$F(\omega)$, $V(\omega)$ or $p(\omega)$
Insertion loss [1,2]	$IL_{Q_i} = 10\log_{10}(\frac{\Psi_{Q_i,A}^2}{\Psi_{Q_i,B}^2})$ dB

Note:
1. Subscripts 1, 2 and 3 are input, interfacial and output locations of components as shown in Fig. 1.
2. Operator '/' is a quotient operation for vectors.
3. Superscripts b and f represent blocked and free boundary conditions at the source output, respectively.
4. Operators $\langle\ \rangle_t$ and diag represent time averaged quantity and diagonal matrix of the original matrix, respectively.
5. Subscripts 'with' and 'without' represent a system with an isolator and without any isolator, respectively. Refer to Figs. 1(b) and (c).
6. Subscripts IN and TR represent input at source and transmitted power at receiver input, respectively.
7. $Q_i = p_i(\omega)$, $F_i(\omega)$ or $V_i(\omega)$ at i. Also, A and B represent two different physical systems.

refers to the case when the source is rigidly connected to the receiver:

$$\Xi_\Pi = \frac{\Pi_{TR,with}}{\Pi_{TR,without}}. \tag{19}$$

Insertion losses (IL) for force and velocity at the receiver structure or sound pressure (p) in the acoustic medium are defined as follows where Ψ^2 is mean-square value of relevant variable Q_i:

$$IL_{Q_i} = 10\log_{10}\left(\frac{\Psi_{Q_i,A}^2}{\Psi_{Q_i,B}^2}\right)\ \mathrm{dB}. \tag{20}$$

One could choose Q_i to be $F_i(\omega)$, $V_i(\omega)$ or $p_i(\omega)$, etc. at location i. Further, A and B represent two different physical systems and therefore the IL values are always relative. The aforementioned vibration isolation measures are summarized in Table 1 for multi-dimensional motions; some explanations are also provided along with citation to literature.

4. System with an inverted 'L' beam receiver

4.1. System configuration

Various vibration isolation measures are examined for an analytical isolation system with the inverted 'L' beam receiver of Fig. 2(a). Note that longitudinal motion of one beam is coupled with flexural motion of the other and thus both contribute to sound radiation. The four isolator attachment cases of Fig. 2(d) are analyzed up to 3 kHz. These cases provide several transmission configurations even though cases 3 and 4 are statically unstable and case 1 is physically meaningful only for three-dimensional motions in terms of its implementation. Nonetheless, vibration transmitted to the receiver is strongly affected by the mount location, and thus by the free velocity of source [12]. Harmonic moment excitations are applied at the mass center of the source for vibratory power-based and sound field measures. Force excitation cases are also examined for transmissibility and effectiveness of force or velocity.

The mobility matrix $\mathbf{M}$ of a rigid body, between any two locations i and j, can be determined from the inertia properties at mass center G and geometric information. Details may be found in Ref. [29]. Using the small angle (θ) approximation ($\sin\theta \approx \tan\theta \approx \theta$ and $\cos\theta \approx 1$), the resulting expressions are given by

$$\begin{bmatrix} \mathbf{V}_i \\ \mathbf{V}_j \end{bmatrix} = \begin{bmatrix} \mathbf{M}_{ii} & \mathbf{M}_{ij} \\ \mathbf{M}_{ji} & \mathbf{M}_{jj} \end{bmatrix} \begin{bmatrix} \mathbf{F}_i \\ \mathbf{F}_j \end{bmatrix} = \begin{bmatrix} \mathbf{T}_i^{\mathrm{T}}\mathbf{M}_{GG}\mathbf{T}_i & \mathbf{T}_i^{\mathrm{T}}\mathbf{M}_{GG}\mathbf{T}_j \\ \mathbf{T}_j^{\mathrm{T}}\mathbf{M}_{GG}\mathbf{T}_i & \mathbf{T}_j^{\mathrm{T}}\mathbf{M}_{GG}\mathbf{T}_j \end{bmatrix} \begin{bmatrix} \mathbf{F}_i \\ \mathbf{F}_j \end{bmatrix}, \tag{21a}$$

$$\mathbf{M}_{GG} = \begin{bmatrix} \mathbf{M}_{v,GG} & 0 \\ 0 & \mathbf{M}_{w,GG} \end{bmatrix}, \tag{21b}$$

$$\mathbf{M}_{v,GG} = \mathrm{diag}\left(\begin{bmatrix} \dfrac{1}{m\mathrm{j}\omega} & \dfrac{1}{m\mathrm{j}\omega} & \dfrac{1}{m\mathrm{j}\omega} \end{bmatrix} \right), \quad \mathbf{M}_{w,GG} = \frac{1}{\mathrm{j}\omega} \begin{bmatrix} I_{m,xx} & -I_{m,xy} & -I_{m,xz} \\ -I_{m,xy} & I_{m,yy} & -I_{m,yz} \\ -I_{m,xz} & -I_{m,yz} & I_{m,zz} \end{bmatrix}^{-1}, \tag{21c, d}$$

$$\mathbf{T}_i = \begin{bmatrix} \mathbf{I} & 0 \\ \mathbf{R}_i & \mathbf{I} \end{bmatrix}, \quad \mathbf{R}_i = \begin{bmatrix} 0 & -h_{zi} & h_{yi} \\ h_{zi} & 0 & -h_{xi} \\ -h_{yi} & h_{xi} & 0 \end{bmatrix}. \tag{21e, f}$$

Here, m and I are mass and inertia of a rigid body and h represents a reference location within the rigid body with respect to G. The isolator is connected to the inverted 'L' beam at $0.75\ell_H$, where ℓ_H is the length of the horizontal beam. This off-center location highlights the effect of coupling mobility of receiver. Note that such a coupling mobility term does not exist for a centrally driven beam (with symmetric boundaries) and for an infinite beam. The isolator of Fig. 2(c) is modelled using the Timoshenko beam theory to describe flexure along with the wave equation for longitudinal motion. Thus, the effects of shear deformation and rotary inertia are included. Mobilities of the Timoshenko beam have been analyzed for two types of solution in an earlier paper by the same authors [21]; the resulting formulations are used here. Material properties such as shear modulus (G), the mass density (ρ) and the Poisson ratio (ν) of the isolator are listed in Table 2. The modulus of elasticity E for the rubber material is found from the relation

Table 2
Material properties and dimensions of the analytical system of Fig. 2(a)

Property or dimension	Source (cubic rigid body)	Isolator (circular beam)	Inverted 'L' beam receiver
m (kg)	1	—	—
E (MPa)	—	16.2	6.688×10^4
G (MPa)	—	5	—
η	—	0.3	0.001
ρ (kg/m^3)	—	1000	2723
Dimensions (mm)	$\ell = 50$	$\ell = 30$ $r = 12$	$\ell = 400$, $b = 100$, $t = 5$ (horizontal and vertical beams)

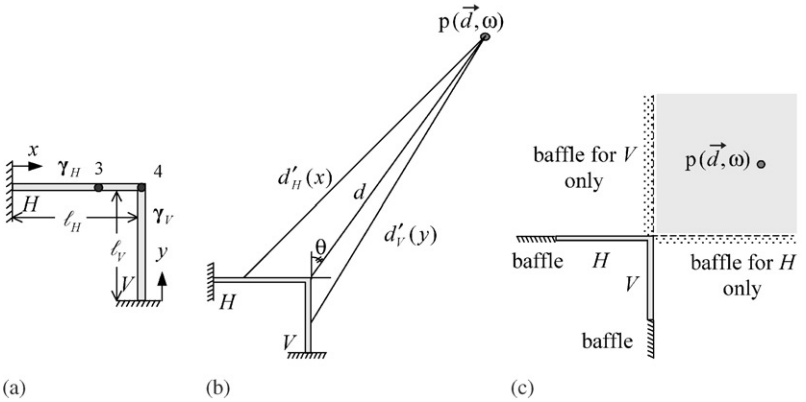

Fig. 3. Sound radiation from an inverted 'L' beam receiver: (a) 'L' beam configuration and its mobilities; (b) acoustic field point. Here, location 3 is interface of receiver with an isolator, and interface between beams H and V is denoted by location 4.

$E = 3G(1 + QT^2)$, where Q is a numerical constant and T is the isolator shape factor [3]. For a circular rubber cylinder, Q is 2 and T is equal to $2r/(4\ell)$, where radius (r) and length (ℓ) values are listed in Table 2 [3]. Also, a frequency-invariant loss factor η of 0.1 is assumed to incorporate damping within the isolator. It is included in the calculation with the complex-valued modulus of elasticity as $\tilde{E} = E(1 + j\eta)$. Also, a loss factor of 0.002 is used to represent a lightly damped structure and included in $\tilde{E}$.

The dynamic behavior of the inverted 'L' beam is obtained by synthesizing the mobilities of each beam. Harmonic responses of the finite beam in flexure are as follows, where k_B is bending wave number and A_B, B_B, C_B and D_B are arbitrary constants:

$$Y(x,t) = Y(x)e^{j\omega t} = \{A_B \sin[k_B x] + B_B \cos[k_B x] + C_B \sinh[k_B x] + D_B \cosh[k_B x]\}e^{j\omega t}. \quad (22)$$

For a horizontal beam (designated as H) with one end clamped and the other end free, the above is rewritten as follows, with reference to Fig. 3(a), when a harmonic force or moment excitation is

applied within the beam span:

$$Y_1(x,t) = Y_1(x)e^{j\omega t} = A_{1B}[\sin[k_B x] - \sinh[k_B x]] + B_{1B}[\cos[k_B x] - \cosh[k_B x]]e^{j\omega t}, \quad (23a)$$

$$Y_2(x,t) = Y_2(x)e^{j\omega t} = A_{2B}[\sin[k_B(\ell_H - x)] + \sinh[k_B(\ell_H - x)]] + B_{2B}[\cos[k_B(\ell_H - x)] + \cosh[k_B(\ell_H - x)]]e^{j\omega t}. \quad (23b)$$

Here, Y_1 and Y_2 are the steady state responses of the beam over spans $0 \leqslant x \leqslant x_F$ and $x_F \leqslant x \leqslant \ell_H$, respectively, where x_F and ℓ_H are the excitation location and length of the horizontal beam, respectively. Unknowns A_{1B}, B_{1B}, A_{2B} and B_{2B} are obtained by applying boundary and excitation conditions. Using the wave equation, the longitudinal velocity of a beam with one end clamped and the other end free is as follows, where k_B and S are longitudinal wave number and section area, respectively [30]:

$$v_{x1}(x,t) = v_{x1}(x)e^{j\omega t} = j\omega \frac{\sin[k_L x]\cos[k_L(\ell_H - x_f)]}{SEk_L \cos[k_L \ell_H]} e^{j\omega t}, \quad 0 \leqslant x \leqslant x_f, \quad (24a)$$

$$v_{x2}(x,t) = v_{x2}(x)e^{j\omega t} = j\omega \frac{\sin[k_L x_f]\cos[k_L(\ell_H - x)]}{SEk_L \cos[k_L \ell_H]} e^{j\omega t}, \quad x_f \leqslant x \leqslant \ell_H, \quad (24b)$$

For a vertical beam of length ℓ_V (designated as V) that is excited at the end of beam, mobilities are also used from Ref. [30] and are not repeated here.

Next, driving point mobilities of inverted 'L' beam at interface with an isolator (location 3) are obtained using the following, where $\boldsymbol{\gamma}_{H,}$ and $\boldsymbol{\gamma}_V$ are the mobilities of horizontal and vertical beams, respectively, as shown in Fig. 2(a), and the subscripts after comma represent related locations:

$$\boldsymbol{\gamma}_{33} = \boldsymbol{\gamma}_{H,,33} - \boldsymbol{\gamma}_{H,,34}[\boldsymbol{\gamma}_{H,,44} + \boldsymbol{\gamma}_{V,,44}]\boldsymbol{\gamma}_{H,43}. \quad (25)$$

Then, interfacial forces $\mathbf{F}_{R3}$ at location 3 are obtained by using Eqs. (1b) and (25) and by employing the same $\boldsymbol{\alpha}$ and $\boldsymbol{\beta}$ for source and isolator, respectively.

4.2. Vibration isolation measures using TR or Ξ

Force and velocity transmissibilities (TR) are computed using the inverted 'L' beam receiver, with only one isolation configuration (case 2) of Fig. 2(d). Only non-dimensional diagonal terms in transmissibility matrices are analyzed. The modified transmissibilities (TR_F^b and TR_V^f) are also compared with their corresponding transmissibilities (TR_F and TR_V) since the TR_F^b and TR_V^f may provide a better or convenient isolation measure. For example, there are cases such as in internal combustion engines where direct force inputs are difficult to measure, and the TR_F^b that employs the blocked force may be considered as an alternative. Further, the effects of free velocity on vibration transmission to receiver have been emphasized for a multi-dimensional isolation system [12] and thus the TR_V^f that employs the free velocity may also be regarded as an important isolation measure for multi-dimensional cases. In such cases, the relationships between the modified and original transmissibilities need to be examined, and the comparison of such transmissibility measures could yield a useful information. First, TR_F and TR_F^b spectra are shown in Fig. 4. The axial and rotational components of TR_F are almost the same as the corresponding components of TR_F^b over the entire frequency range. The lateral components of TR_F and TR_F^b

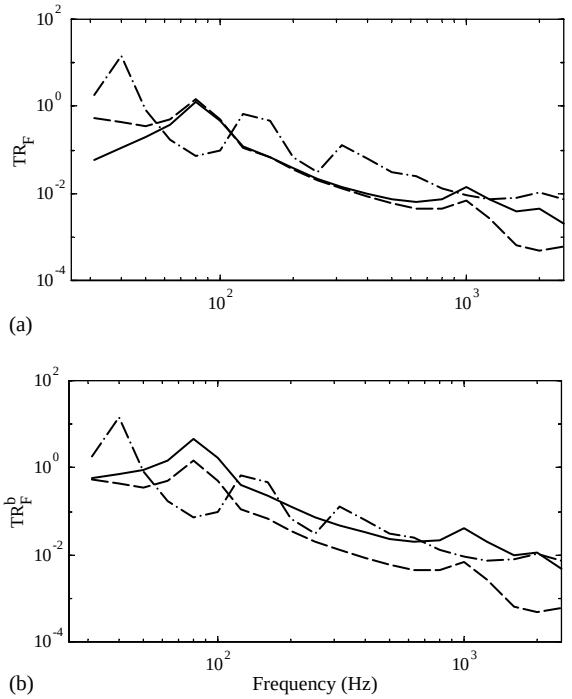

Fig. 4. Force transmissibility with an inverted 'L' beam receiver and case 2 isolator: (a) force transmissibility TR_F; (b) modified force transmissibility TR_F^b. ——, f_x; – – – – –, f_y; - - - - - - -, q_z.

also have almost the same spectral shapes but the lateral TR_F^b is higher than the one of TR_F. Therefore, TR_F^b may be regarded as an alternative to TR_F for some cases (axial and rotational components in this case) although one must exercise caution when replacing of TR_F^b by TR_F.

Next, the velocity TR_V and modified velocity TR_V^f transmissibilities are shown in Fig. 5. The differences between the TR_V and TR_V^f components are more pronounced than the ones between TR_F and TR_F^b. This is because the axial components of TR_V and TR_V^f dominate over the entire frequency range and the lateral components of TR_V and TR_V^f are higher than the rotational component of those. Also, the difference between lateral and rotational components is reduced in the TR_V^f calculations.

Finally, the Ξ_F and Ξ_V effectiveness spectra are shown in Fig. 6. Unlike the TR_V and TR_V^f, the lateral and rotational components of Ξ_V are almost the same and the lateral component of Ξ_F is slightly larger than the rotational component of Ξ_F up to around 400 Hz, as shown in Fig. 6. Therefore, the difference between TR_V and Ξ_V confirms that the TR_V does not properly represent the isolation effectiveness for the different motional directions, as known previously. However, similar to TR_V and TR_V^f, it is observed that the axial component of Ξ_F or Ξ_V dominates beyond 100 Hz.

4.3. Power-based vibration isolation measures

The four different cases of the isolator connection, as shown in Fig. 2(d), are investigated using the same component parameters. Vibration power transmitted to the receiver is computed and

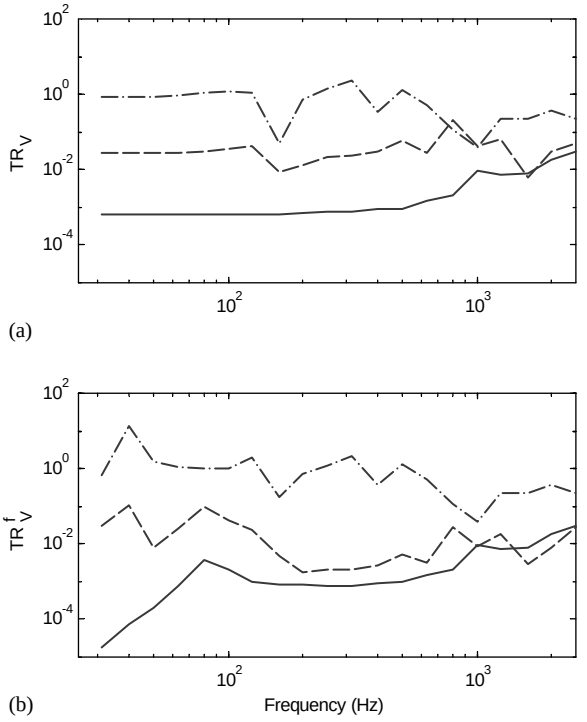

Fig. 5. Velocity transmissibility with an inverted 'L' beam receiver and case 2 isolator: (a) velocity transmissibility TR_V; (b) modified velocity transmissibility TR^f_V. ——, v_x; – – – – –, v_y; - - - - - - -, w_z.

analyzed up to 3 kHz. As mentioned earlier, each power component cannot be decoupled from others because of coupling and therefore may be positive or negative. Vibration power components (Π) that are normalized with respect to the total power (Π_{Total}) transmitted to the inverted 'L' beam are shown in Fig. 7. Therefore, the normalized power components shown in this manner add up to unity. However, it is seen from Fig. 7 that the normalized Πs exceed far from unity because of coupling and exhibit somewhat complicated characteristics of the power transmission process. Note that for the inverted 'L' beam receiver, the longitudinal motion of beam H is coupled with the rotational motion of beam V, ultimately with bending motion of the horizontal beam. Therefore, all coupling terms in the driving point mobility of the 'L' beam receiver are non-zero and coupling powers exist between lateral (with respect to isolator) and other directions. However, the coupling does not occur between longitudinal and other (bending) directions of a single straight beam receiver. Fig. 7 shows that the rotational Π_R is dominant and large negative power flows in the axial y (with respect to isolator) direction are observed for cases 1 and 2. This implies that there exists Π flow from a receiver to an isolator in the axial direction. Further, the lateral Π_ℓ of case 2 grows at higher frequencies. For cases 3 and 4, the axial Π_A is dominant except certain frequencies (around 1 kHz), as shown in Figs. 7(c) and (d). At these frequencies in cases 3 and 4, the Π_R dominates and the Π_A flows in reverse manner (from a receiver to an isolator). Overall, Fig. 7 shows that the Π_A and Π_R spectra are almost symmetric with respect to $\Pi/\Pi_{Total} = 0.5$. This indicates that significant coupling occurs between the Π_A (shear direction of horizontal beam receiver) and Π_R components. Although parts of these

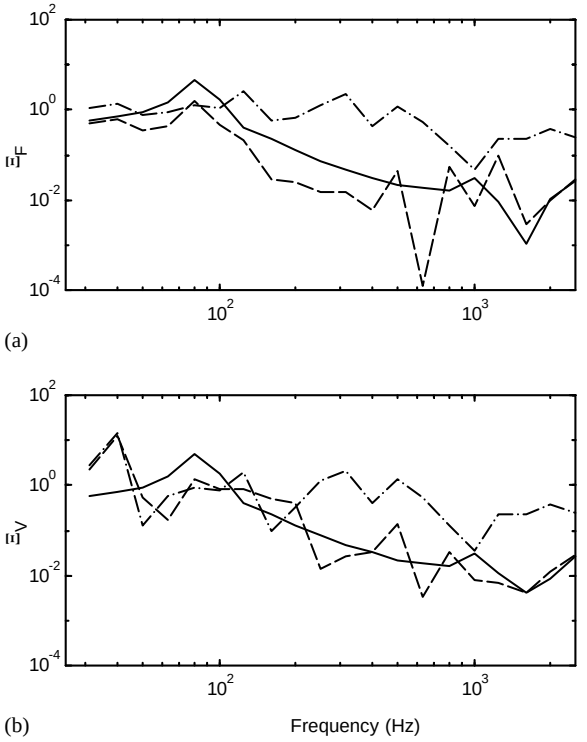

Fig. 6. Force and velocity effectiveness with an inverted 'L' beam receiver and case 2 isolator: (a) force effectiveness Ξ_F; (b) velocity effectiveness Ξ_V. ——, f_x; – – – – –, f_y; - - - - - - -, q_z.

components ultimately cancel each other, all of these orthogonal components may be separately considered in the analysis. For example, consider a system consisting of multiple uni-directional paths. Like the case considered here, reverse (negative) Π flows are expected to occur within certain paths and frequencies since the transfer mobility can be positive or negative. Despite the cancellation of coupling powers within some paths, negative or positive power flow through each uni-directional path must be separately understood to properly design a vibration isolation system for minimum structure-borne noise. Likewise, each path of a multi-dimensional isolator may be analyzed independently. However, it may be useful to group and compare powers for the sake of interpretation. For example, shear and rotational motions are associated with each other by the relationship $w = \mathrm{d}v/\mathrm{d}x$ and $f = -\mathrm{d}q/\mathrm{d}x$ for a beam structure where v, w, f and q represent translational and rotational velocities, force and moment, respectively. Therefore, in our study, the bending Π_B is defined as the sum of the Π_A and Π_R components and it is compared with the Π_ℓ in Fig. 8. The Π_B represents the powers in flexural motion of beam H. However, it should be noted that, in general, this description of flexural motion is not appropriate since the receiver dynamics is governed not only by a directly connected structure but also by subsequent structures. Fig. 8(a) shows that the Π_B is dominant except around 300 Hz and the Π_ℓ flows upward to an isolator at higher ω for case 1. Further, the Π_B and Π_ℓ dominate at lower and higher frequencies respectively for case 2, and the Π_B dominates at all frequencies for cases 3 and 4, as shown in Fig. 8(b). The negative Π_ℓ values of Fig. 8 indicate the existence of the coupling between

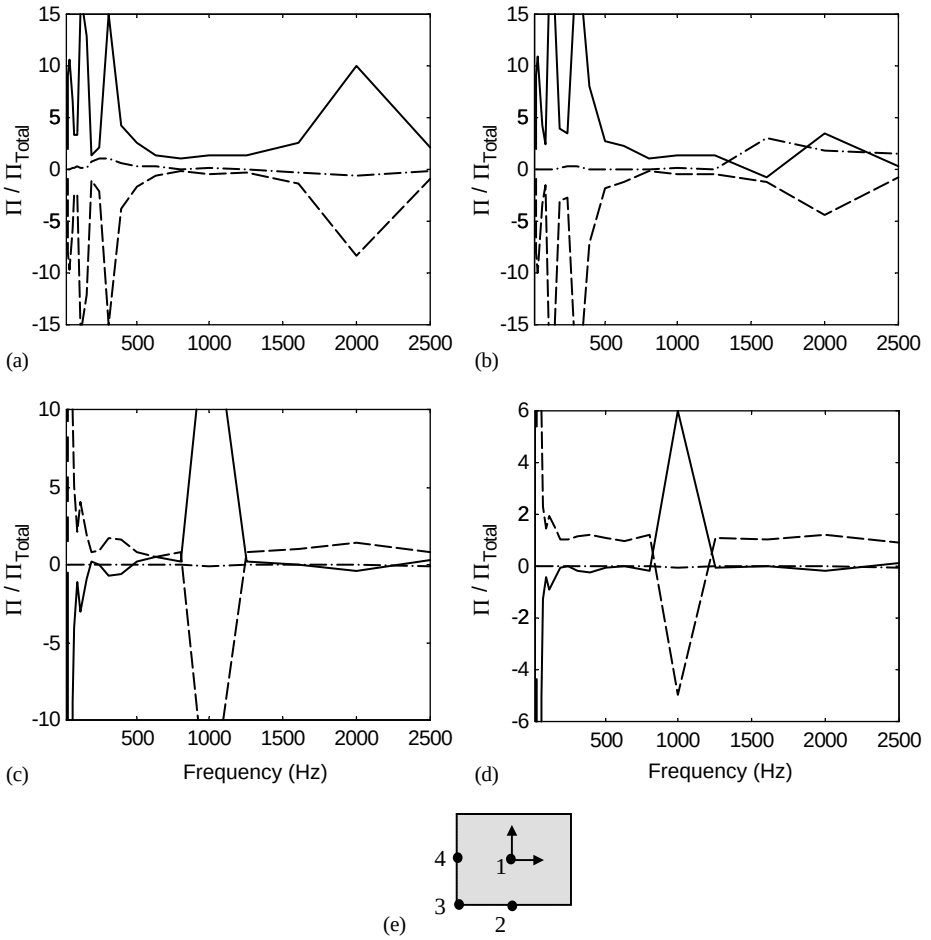

Fig. 7. Normalized vibration power component with respect to the total power transmitted to an inverted 'L' beam receiver given moment excitation: (a) case 1; (b) case 2; (c) case 3; (d) case 4 as shown in Fig. 2(d); (e) four mounting location cases as shown in Fig. 2(d). -------, axial; ——, rotational; – – – – -, lateral.

longitudinal and bending motions of the 'L' beam receiver. As mentioned previously, the Π_ℓ cannot be negative for a system with a single straight beam receiver. Overall, it can be seen from Fig. 8 that strong coupling still exists between bending and lateral directions due to interactions between receiver structures. In this study, the vibration transmission paths could be identified in a more clear manner by grouping the power components in flexural motions. But, caution must be exercised since the longitudinal motion of a receiver may exhibit strong coupling with its bending motions unlike the 'L' beam case examined here. For example, the bending waves through an isolator are typically converted to the longitudinal wave of a receiver, and grouping of flexural motions of an isolator rather than the ones of a receiver may be more suitable in some application. Future research should attempt to properly interpret the vibration transmission process and related couplings, and an efficient analysis scheme must be sought via a better understanding of the coupling process.

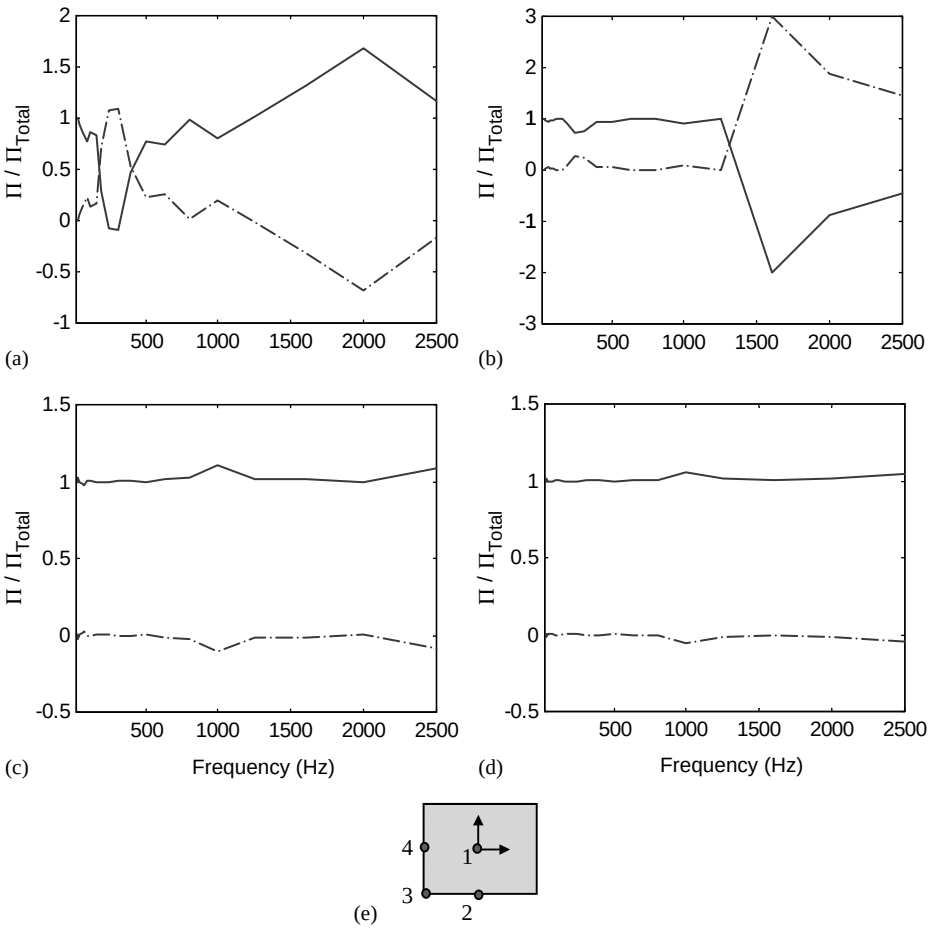

Fig. 8. Normalized vibration power component with respect to the total power transmitted to an inverted 'L' beam receiver given moment excitation: (a) case 1; (b) case 2; (c) case 3; (d) case 4 as shown in Fig. 2(d); (e) four mounting location cases as shown in Fig. 2(d). ——, bending; – – – – –, lateral.

Next, the weighted mean square force (Ψ^2_{WF}) and coupling power that are normalized with respect to Π_{Total} are calculated and shown in Fig. 9. Recall from Section 3.4, that the coupling power is designated as the sum of the power terms consisting of a force (or moment) and velocity that is generated by the forces (or moments) in different directions. Further, the sum of the $\Psi^2_{WF,Total}$ (or $\Psi^2_{WV,Total}$) and the coupling power is equal to the total power (Π_{Total}) transmitted to the receiver. Fig. 9 shows that the rotational and axial Ψ^2_{WF} are dominant for cases 1 and 2 and the axial Ψ^2_{WF} dominates for cases 3 and 4. Further, the lateral Ψ^2_{WF} becomes important as frequency increases for case 2, like the Π spectra in Fig. 8(b). The Ψ^2_{WF} of Fig. 9 also exhibits strong power coupling phenomena. However, Ψ^2_{WF} does not provide any information on power flowing in the reverse manner as seen in the Π spectra since Ψ^2_{WF} is always positive. This can be seen from the coupling power. The weighted mean-square velocity (Ψ^2_{WV}) is also shown in Fig. 10. The Ψ^2_{WV} spectra are quite different from the Ψ^2_{WF} for all cases. Note that Ψ^2_{WF} and Ψ^2_{WV} are the same when a receiver is defined only in terms of a diagonal driving point mobility matrix such as

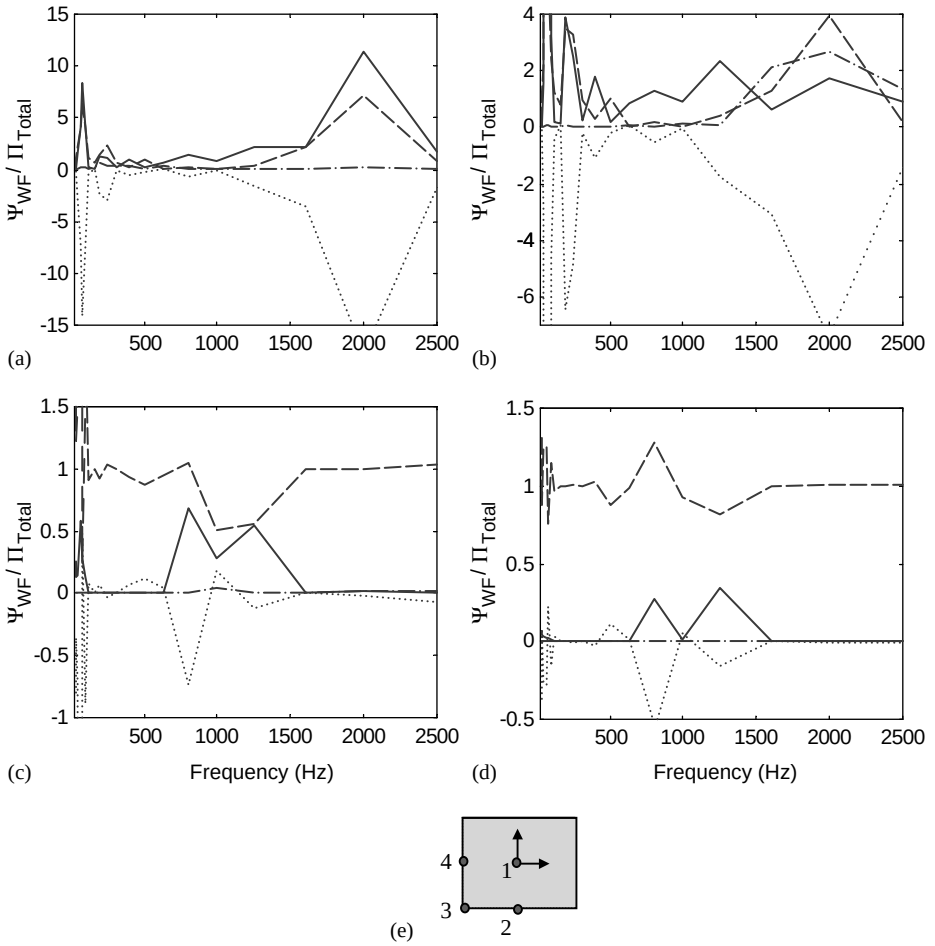

Fig. 9. Weighted mean square force (Ψ^2_{WF}) and coupling power normalized with respect to the total power transmitted to an inverted 'L' beam receiver given moment excitation: (a) case 1; (b) case 2; (c) case 3; (d) case 4 as shown in Fig. 2(d); (e) four mounting location cases as shown in Fig. 2(d). -------, axial; ——, rotational; – – – –, lateral; ……, coupling power.

an infinite beam or a finite beam (with symmetric boundaries) with the isolator connected at the center. Like the Ψ^2_{WF}, Fig. 10 shows that the rotational and axial Ψ^2_{WV}'s are significant for all cases. However, the lateral Ψ^2_{WV} becomes important over a relatively limited frequency range. Further, stronger coupling terms are observed in Fig. 10 than in Fig. 9.

Total vibration powers Π_{Total} transmitted to the 'L' beam receiver are compared in Fig. 11(a) for the 4 location cases of Fig. 2(d) given unit (1 N m) moment excitation. It is observed that total vibration powers for cases 3 and 4 are almost the same but these are higher than those for cases 1 and 2. Also, the transmitted power is lowest among the cases considered when the isolator is attached to the mass center of the rigid body (case 1). The power efficiencies Γ are shown in Fig. 11(b), and a rank order based on Γ is similar to the one given by Π_{Total}. However, Γ in case 1 rises and is higher than the one for case 2 as ω increases. Also, for all cases, overall characteristics

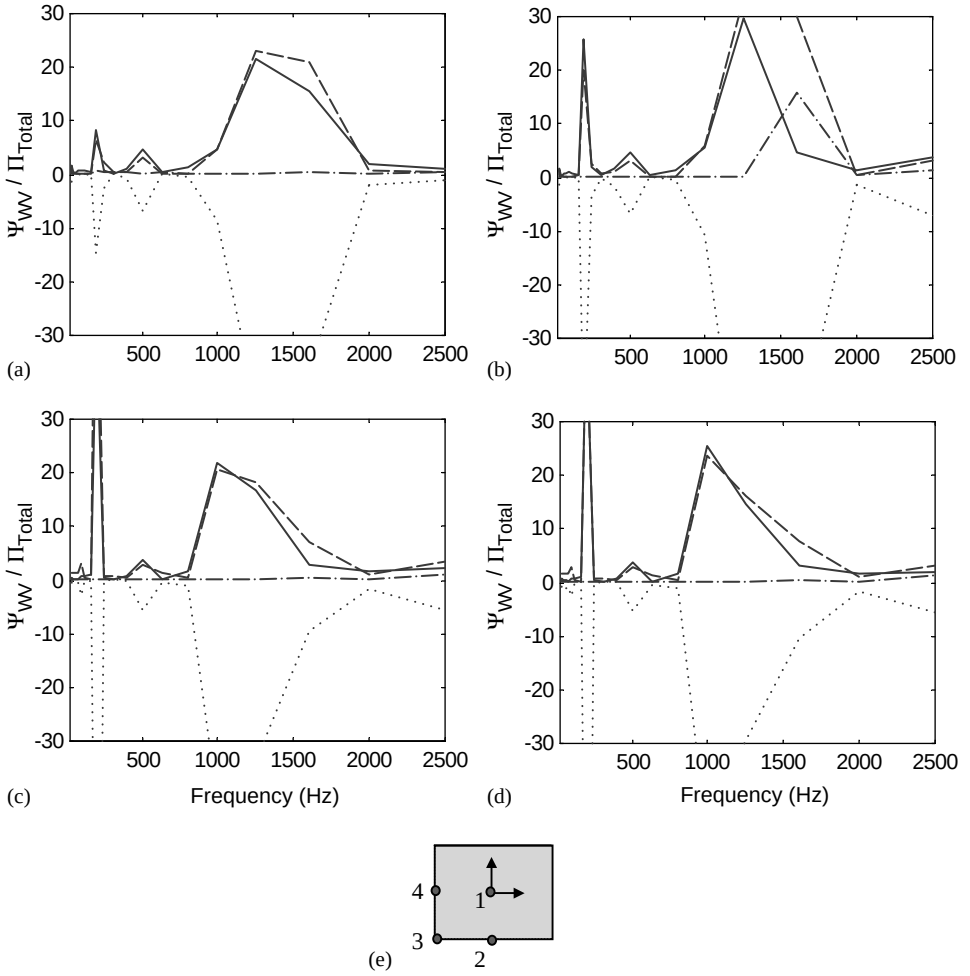

Fig. 10. Weighted mean square velocity (Ψ^2_{WV}) and coupling power normalized with respect to the total power transmitted to an inverted 'L' beam receiver given moment excitation: (a) case 1; (b) case 2; (c) case 3; (d) case 4 as shown in Fig. 2(d); (e) four mounting location cases as shown in Fig. 2(d). -------, axial; ——, rotational; – – – – –, lateral; ……, coupling power.

of Γ rise as ω increases even though the value of Π_{Total} decreases. The power effectivenesses Ξ_{Π} are also shown in Fig. 11(c). The patterns for Ξ_{Π} spectra do not exactly match with Π_{Total} for the cases considered. For example, The Ξ_{Π} for case 3 is higher than the one of case 4 at low frequencies but is lower at high ω. Overall, one must properly select a power-based measure, given the choice between force (or velocity) transmissibility and effectiveness terms. Further, the differences between Π_{Total} and Γ are expected since the source input powers of each case are different although the excitation moment amplitude remains unchanged. Therefore, the source characteristics also need to be identified to examine various design modifications. For example, Γ is suitable when a source generating mechanism is clearly identified. Without a proper understanding of such a source, Π_{Total} must be evaluated for each design change.

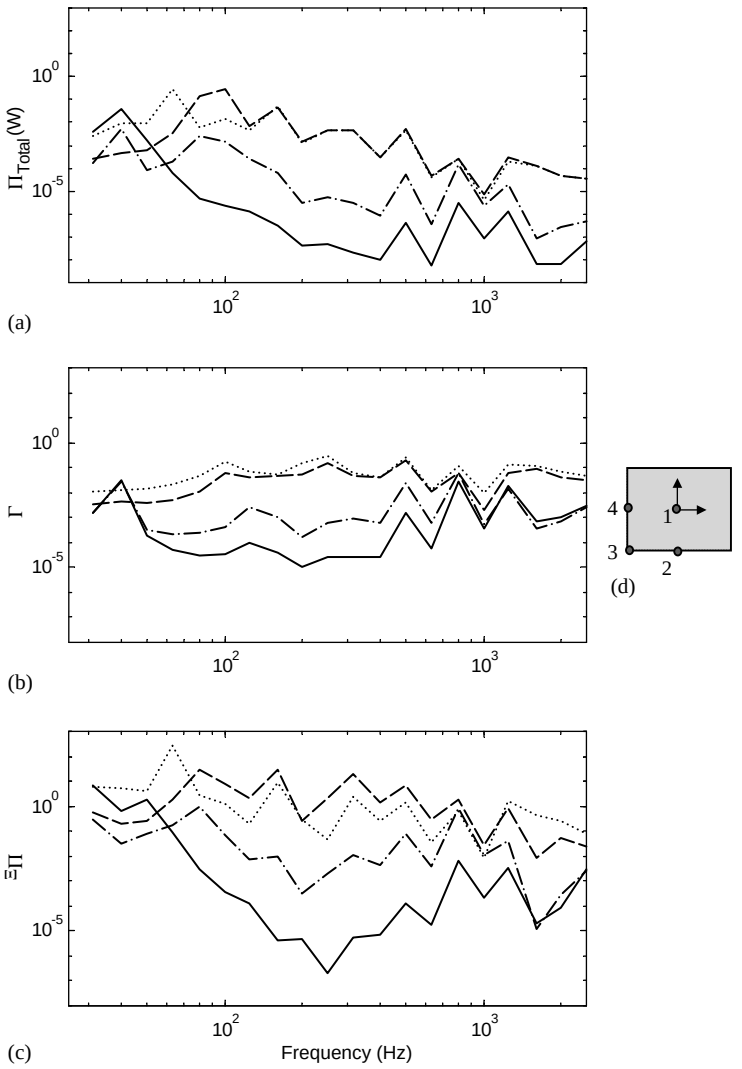

Fig. 11. Vibration isolation measures with an inverted 'L' beam receiver given moment excitation: (a) total transmitted vibration power Π_{Total}; (b) efficiency Γ for total transmitted vibration power; (c) effectiveness Ξ_Π for total transmitted vibration power; (d) four mounting location cases as shown in Fig. 2(d). ——, mount location case 1; – – – –, case 2; - - - - - - -, case 3; ·····, case 4.

4.4. Sound radiation from receiver as a measure of vibration isolation

Sound pressure p at selected points in free field ($\vec{d}$) is calculated in order to examine its relationship with vibration power transmitted to the receiver of Fig. 2(a). An inverted 'L' beam is chosen as the chief radiating structure and it will incorporate contributions from longitudinal and flexural structural powers. See Fig. 3 for more details of the system configuration. First, interfacial forces $\mathbf{F}_{R4}$ between horizontal (H) and vertical (V) beams are obtained by using $\mathbf{F}_{R3}$

as follows:

$$\mathbf{F}_{R4} = [\boldsymbol{\gamma}_{H,,44} + \boldsymbol{\gamma}_{V,,44}]^{-1}\boldsymbol{\gamma}_{H,43}\mathbf{F}_{R3}. \tag{26}$$

Further, velocity distributions along x and y of beams H and V can be represented as follows:

$$\mathbf{V}_H(x) = \boldsymbol{\gamma}_{H,x3}(x)\mathbf{F}_{R3} + \boldsymbol{\gamma}_{H,x4}(x)\mathbf{F}_{R4}, \tag{27a}$$

$$\mathbf{V}_V(y) = \boldsymbol{\gamma}_{V,y4}(y)\mathbf{F}_{R4}. \tag{27b}$$

Assume distributed line source on the beams, and the sound pressure at $\vec{d}$ from a baffled harmonic source is [31,32]

$$p = \int_0^L \left[\frac{\mathrm{j}\rho_a c_a k_a}{2\pi d'(x)}\, v(x) b \mathrm{e}^{\mathrm{j}[\omega t - k_a d'(x)]}\right] \mathrm{d}x. \tag{28}$$

Here, d' is a distance between the vibrating point on the beam and the observation point $\vec{d}$, b is the beam width and ρ_a, c_a and k_a are the density, wave speed and wave number of the air medium, respectively. Assuming a far field, such that $d \gg \ell$, where d is the reference location at the intersection of two beams in this case, d'_H and d'_V can be approximated as

$$d'_H(x) \approx d + (\ell_H - x)\sin\theta, \quad d'_V(y) \approx d + (\ell_V - y)\cos\theta. \tag{29a, b}$$

Further, d'_H and d'_V in the denominator of the integrand can be replaced by its approximate value d but not for the exponent in order to maintain the phasing relations [31]. Here, the sound field in the second quarter of Fig. 3(c) is described by a superposition of two independent hemi-spherical spaces corresponding to the horizontal and vertical baffled beam radiators, as shown in Fig. 3. Note that the Green's function for a $\frac{3}{4}$ free space is needed to describe the exact sound field and hence there may exist a discrepancy between the realistic sound field and the one described here especially at lower frequencies. Consequently, this study focuses on relative measures of two different systems, such as the insertion loss, and accordingly it is assumed that such discrepancies are negligible especially in the sound field located 45° from the corner of the beams. Yet, a more general case that employs an inverted 'L' plate and describes a three-dimensional sound field is investigated via computational and experimental studies in Section 5. Therefore, sound pressure contributions from beams H and V are

$$p = p_H + p_V, \tag{30a}$$

$$p_H = \frac{\mathrm{j}\rho_a c_a k_a \ell_{p,H}}{4\pi d}\, \mathrm{e}^{\mathrm{j}[\omega t - k_a(d-\ell_H)]} \int_0^{\ell_H} v_{H,y}(x) \mathrm{e}^{\mathrm{j}k_a x \sin\theta}\, \mathrm{d}x, \tag{30b}$$

$$p_V = \frac{\mathrm{j}\rho_a c_a k_a \ell_{p,V}}{4\pi d}\, \mathrm{e}^{\mathrm{j}[\omega t - k_a(d-\ell_V)]} \int_0^{\ell_V} v_{V,x}(y) \mathrm{e}^{\mathrm{j}k_a y \cos\theta}\, \mathrm{d}y. \tag{30c}$$

Here, $v_{H,y}$ and $v_{V,x}$ are the flexural velocities of beams H and V, respectively. Sound pressure from beam H is determined as follows where $\mathbf{G}$ is a row vector:

$$p_H = \frac{\mathrm{j}\rho_a c_a k_a \ell_{p,H}}{4\pi d}\, \mathrm{e}^{\mathrm{j}[\omega t - k_a(d-\ell_H)]}[\mathbf{G}_{H1,3}\mathbf{F}_3 + \mathbf{G}_{H2,3}\mathbf{F}_3 + \mathbf{G}_{H1,4}\mathbf{F}_4], \tag{31a}$$

$$\mathbf{G}_{H1,3} = [A_{H1,v_x}(x_3) \quad A_{H1,v_y}(x_3) \quad A_{H1,q_z}(x_3)]g_{H1,A} + [B_{H1,v_x}(x_3) \quad B_{H1,v_y}(x_3) \quad B_{H1,q_z}(x_3)]g_{H1,B}, \tag{31b}$$

$$\mathbf{G}_{H2,3} = [A_{H2,v_x}(x_3) \quad A_{H2,v_y}(x_3) \quad A_{H2,q_z}(x_3)]g_{H2,A} + [B_{H2,v_x}(x_3) \quad B_{H2,v_y}(x_3) \quad B_{H2,q_z}(x_3)]g_{H2,B}, \tag{31c}$$

$$\mathbf{G}_{H1,4} = [A_{H1,v_x}(\ell_H) \quad A_{H1,v_y}(\ell_H) \quad A_{H1,q_z}(\ell_H)]g_{H1,A} + [B_{H1,v_x}(\ell_H) \quad B_{H1,v_y}(\ell_H) \quad B_{H1,q_z}(\ell_H)]g_{H1,B}, \tag{31d}$$

$$g_{H1,A} = \int_0^{x_3} [\sin(k_H x) - \sinh(k_H x)]\mathrm{e}^{\mathrm{j}k_a x \sin\theta}\,\mathrm{d}x, \tag{31e}$$

$$g_{H1,B} = \int_0^{x_3} [\cos(k_H x) - \cosh(k_H x)]\mathrm{e}^{\mathrm{j}k_a x \sin\theta}\mathrm{d}x, \tag{31f}$$

$$g_{H2,A} = \int_{x_3}^{\ell_H} [\sin[k_H(\ell_H - x)] + \sinh[k_H(\ell_H - x)]]\mathrm{e}^{\mathrm{j}k_a x \sin\theta}\,\mathrm{d}x, \tag{31g}$$

$$g_{H2,B} = \int_{x_3}^{\ell_H} [\cos[k_H(\ell_H - x)] + \cosh[k_H(\ell_H - x)]]\mathrm{e}^{\mathrm{j}k_a x \sin\theta}\,\mathrm{d}x. \tag{31h}$$

Similarly, sound pressure from beam V is

$$p_V = \frac{\mathrm{j}\rho_a c_a k_a \ell_{p,V}}{4\pi d}\,\mathrm{e}^{\mathrm{j}[\omega t - k_a(d-\ell_V)]}[\mathbf{G}_{V,4}\mathbf{F}_4], \tag{32a}$$

$$\mathbf{G}_{V,4} = [A_{V,v_x}(\ell_V) \quad A_{V,v_y}(\ell_V) \quad A_{V,q_z}(\ell_V)]g_{V,A} + [B_{V,v_x}(\ell_V) \quad B_{V,v_y}(\ell_V) \quad B_{V,q_z}(\ell_V)]g_{V,B}, \tag{32b}$$

$$g_{V,A} = \int_0^{\ell_V} [\sin(k_V x) - \sinh(k_V x)]\mathrm{e}^{\mathrm{j}k_a y \cos\theta}\,\mathrm{d}y, \tag{32c}$$

$$g_{V,B} = \int_0^{\ell_V} [\cos(k_V x) - \cosh(k_V x)]\mathrm{e}^{\mathrm{j}k_a y \cos\theta}\,\mathrm{d}y. \tag{32d}$$

Calculated mean-square sound pressures (Ψ_p^2) are shown in Fig. 12(a) for four cases. The horizontal beam is connected to the isolator at $3\ell_H/4$ from its clamped end. The field point is located at $d = 1$ m from the intersection of two beams, at 45° from the outer surfaces of each beam, as shown in Fig. 3(b). The rank order associated with four locations and related sound pressure spectral shapes of Fig. 12(a) match the transmitted vibration power spectra of Fig. 11(a) although discrepancies are observed at some frequencies. Sound pressures at other field observation points, $d = 3$ m with 45° and $d = 1$ m with 85°, are also shown in Figs. 12(b) and (c). It is observed from Fig. 12 that the rank orders (corresponding to four isolator locations) at different sound field observation points do not change, except at some frequencies although their spectral shapes differ especially beyond 200 Hz. Fig. 13 compares insertion losses based on mean-squared sound pressures ($IL_{\psi_p^2,i-j}$) at a field point ($d = d_1$, $\theta = \theta_1$) with the ones of vibration power

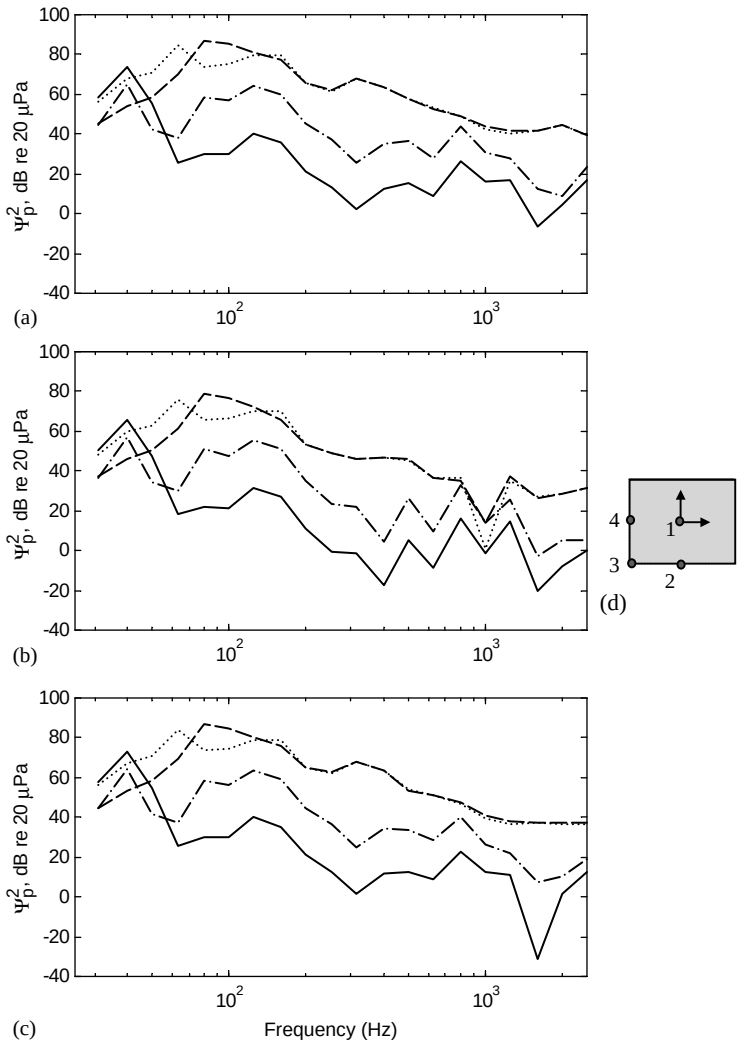

Fig. 12. Far field sound pressures radiated by the 'L' beam of Fig. 3. (a) sound pressure location $d = d_1$, $\theta = \theta_1$; (b) $d = 3d_1$, $\theta = \theta_1$; (c) $d = d_1$, $\theta = \theta_1 + \Delta\theta$; (d) four mounting location cases as shown in Fig. 2(d). ——, mount location case 1; – – – – –, case 2; - - - - - - -, case 3; ·····, case 4.

input ($IL_{\Pi,i-j}$) to the 'L' beam for the four isolator cases of Fig. 2(d) given the moment excitation. Here, subscripts i and j denote mount cases as shown in Fig. 2(d). Spectral averages of the insertion losses ($IL_{\psi_p^2,SAvg}$ and $IL_{\Pi,SAvg}$) are also compared in Fig. 13. Fig. 13 shows that the $IL_{\psi_p^2}$ spectra closely represent the IL_{Π} curves although some discrepancies between $IL_{\psi_p^2,4-1}$ and $IL_{\Pi,4-1}$ (cases 4 and 1) are observed. This suggests that $IL_{\psi_p^2,i-j}$ may not be equal to $IL_{\Pi,i-j}$ when systems i and j transmit different vibration components. Note that the rotational and axial components dominate the vibration transmission for cases 1 and 4, respectively. Therefore, in such cases, correlations between $IL_{\psi_p^2}$ and IL_{Π} could be enhanced by averaging sound pressures over the entire field.

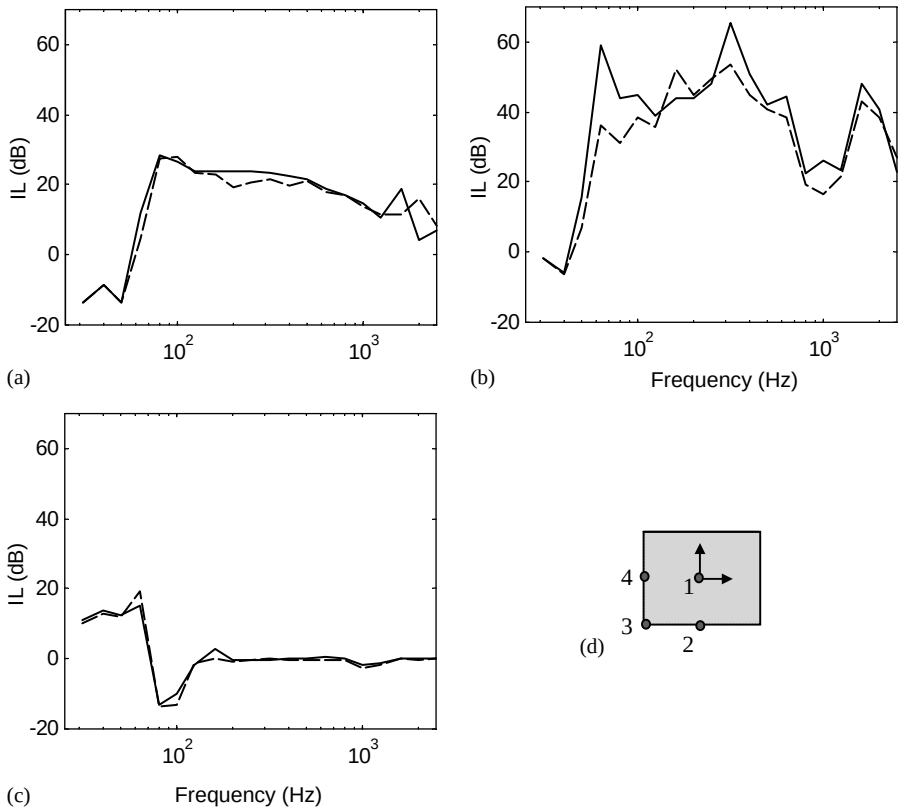

Fig. 13. Insertion losses of mean square sound pressure ($IL_{\psi_p^2}$) at $d = d_1$, $\theta = \theta_1$ and vibration power input (IL_{Π}) to the 'L' beam given moment excitation for four cases as shown in Fig. 2(d). (a) IL_{2-1} (case 2–case 1) with spectral averages of $IL_{\psi_p^2,SAvg} = 14.3$ dB, $IL_{\Pi,SAvg} = 13.5$ dB; (b) IL_{4-1} (case 4–case 1) with $IL_{\psi_p^2,SAvg} = 35.9$ dB, $IL_{\Pi,SAvg} = 31.5$ dB; (c) IL_{4-3} (case 4–case 3) with $IL_{\psi_p^2,SAvg} = 1.0$ dB, $IL_{\Pi,SAvg} = 1.4$ dB; (d) four mounting location cases as shown in Fig. 2(d). ——, $IL_{\psi_p^2}$; - - - - - - -, IL_{Π}. Here, subscript $SAvg$ implies spectral average of corresponding insertion losses.

5. Experimental system with an inverted 'L' plate receiver

5.1. System configuration

Similar to the inverted 'L' beam receiver, an inverted 'L' plate receiver, as shown in Fig. 14, is employed to describe both in-plane and out-of-plane motion transmissions to the receiver. Overall, 4 isolators of Figs. 14(c) and (d) are experimentally studied. The material properties and dimensions of the source, isolator and receiver are summarized in Table 3. Each isolator is located at either the center or edge of mass to realize different vibration isolation configurations. However, the mount location on the receiver side is unchanged. The field point ($\xi_1 = \vec{d}$) for sound pressure measurements $p(\omega)$ is located at a distance of 0.2 m from the mating edge of two plates, at 45° from the outer surfaces. Sound pressures at other field locations (ξ) and structural velocities at selected points (ξ) on the receiver plates are also examined, as summarized in Table 4. Fig. 15 shows the modified experimental schematic used for moment driven responses where a phase shifter is used. Table 5 lists the instruments used. Measurement are conducted in an anechoic

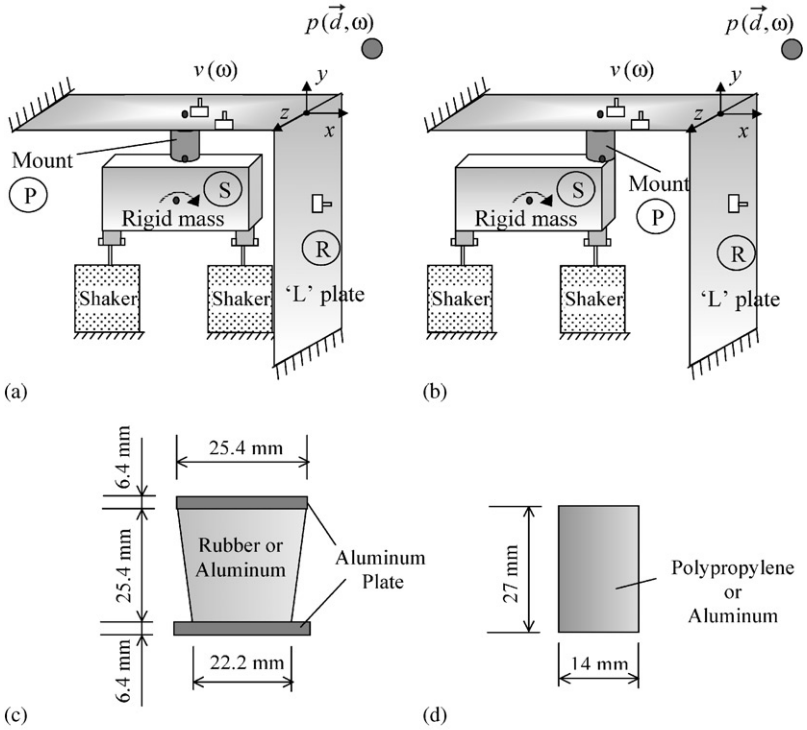

Fig. 14. Experimental system with an inverted 'L' plate receiver, as excited by harmonic forces and moment: (a) system with rotational free velocity only; (b) system with translational and rotational free velocities; (c) isolator I; (d) isolator II.

Table 3
Material properties and dimensions of the experimental system of Fig. 13

Property or dimension	m (kg)	E (MPa)	G (MPa)	η	ρ (kg/m^3)	Dimensions (mm)
Source (rectangular rigid body)	1.2	—	—	—	—	$\ell = [x, y, z] = [140, 64, 47]$
Rubber isolator I	—	2.8	0.8	0.2	1000	$\ell_{effective} = 35$ $r_{effective} = 12$
Aluminum isolator I	—	6.688×10^4	2.4×10^4	0.001	2723	$\ell_{effective} = 35$ $r_{effective} = 12$
Polypropylene isolator II	—	5	1.6	0.2	1000	$\ell = 27$ $r = 7$
Aluminum isolator II	—	6.688×10^4	2.4×10^4	0.001	2723	$\ell = 27$ $r = 7$
Inverted 'L' plate receiver	—	19.5×10^4	8.3×10^4	0.001	7700	$\ell = 400$ $t = 1$ (square horizontal and vertical plates)

Note that rubber and polypropylene properties are approximate.

room under the sine sweep excitation (up to 3 kHz). In-phase and 180° out-of-phase forces (in y direction) are separately applied to the edges of the rigid source to simulate the force (f_y) and moment (q_z) excitations at G, respectively. Forces from two shakers and accelerations at the driving point locations are measured using two impedance heads. Plastic and steel stingers are

Table 4
Locations of vibration transmission measures

Location no.	Measure	Co-ordinates (m)	'L' structure location
ξ_1	Sound pressure	$x = 0.14$, $y = 0.14$, $z = 0$	Acoustic free field
ξ_2	Sound pressure	$x = -0.18$, $y = 0.46$, $z = 0$	Acoustic free field
ξ_3	Velocity	$x = -0.15$, $y = 0$, $z = 0$	Horizontal plate
ξ_4	Velocity	$x = 0$, $y = -0.15$, $z = 0$	Vertical plate

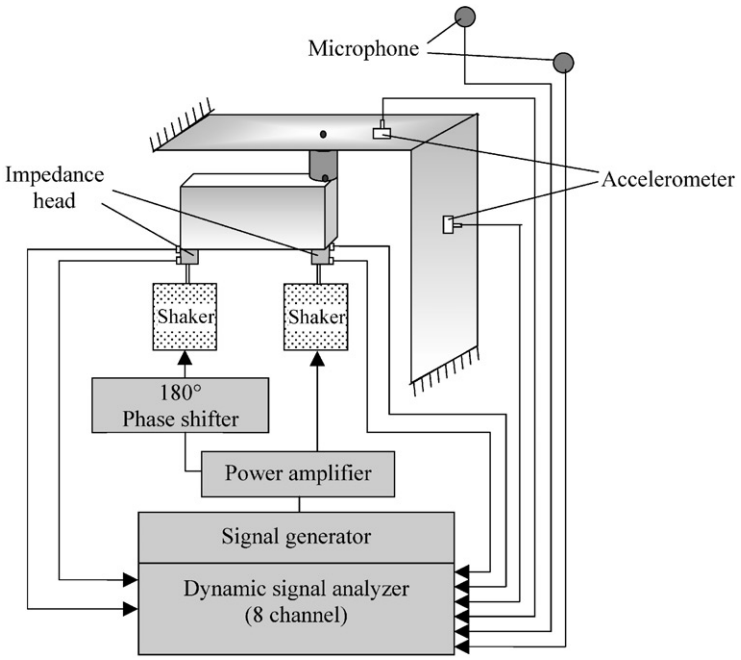

Fig. 15. Experimental schematic for the source characteristics study of a system with an inverted 'L' plate receiver and sound radiated from receiver plate.

Table 5
List of instruments used for experimental studies

Item	Manufacturer	Model no.
Accelerometers	PCB	A353B66
Microphones	PCB	L130C10
Impedance heads	PCB	288D01
Shakers	Labworks	ET-132-2
Phase shifter	AVC Instrumentation	780M01
Power amplifiers	Electro-Voice	7300A
Dynamic signal analyzer (8 channel) with signal generator	HP	HP3566A

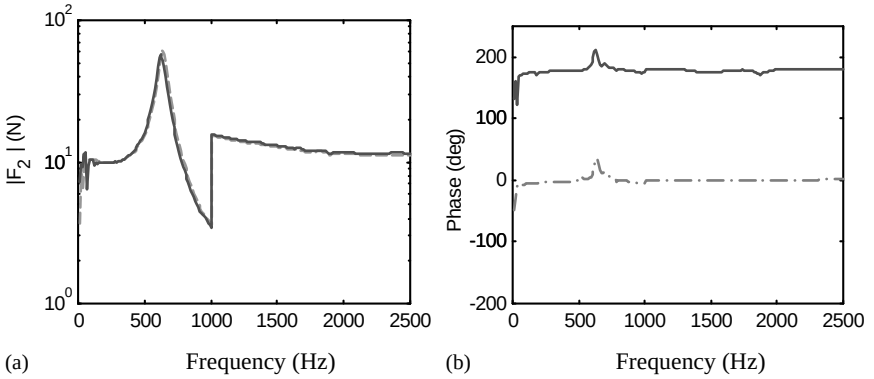

Fig. 16. Typical force input to the mass source. (a) Force magnitude: ——, mount located at the edge of source; – - – - –, mount located at the center of source. (b) Relative phase between two force inputs. ——, moment excitation; – - – - –, force excitation.

used over low (up to 1 kHz) and high (1–3 kHz) frequency regimes, respectively, since the dynamic forces could not excite the system above 1 kHz with plastic stingers. Typical force signals are shown in Fig. 16. The input forces with almost the same magnitudes and 180° (or 0°) phase difference are maintained throughout the experiments for moment (or force) excitation cases as shown in Fig. 17. However, the phase between two forces deviates slightly from 180° (or 0°) at a system resonance (approximately 600 Hz). This resonance appears to be a result of the experimental system dynamics with two shakers. Forces measured at the driving point locations are used for computational predictions.

The mobilities of the inverted 'L' plate structure are obtained by using a commercial finite element (FEA) IDEAS [33] code. Further, interfacial forces and moments between the isolator and receiver are calculated by synthesizing the mobilities of the inverted 'L' plate, source and isolator. Then, the plate velocity distribution from the FEA calculation is provided to a commercial boundary element method (BEM) SYSNOISE [34] code to predict the sound radiation. Individual sound fields generated by each plate for interfacial forces and moments are superimposed to determine the resultant sound pressure. Note that direct radiation from either source or isolator is not included in such calculations. Overall, sound pressure and velocity amplitudes at locations of Table 4 are obtained using the FEA and BEM methods. Vibration power (Π_{TR}) transmitted to the 'L' plate and the power (Π_{RAD}) radiated to the acoustic medium from the receiver, as defined below, are also predicted:

$$\Pi_{RAD} = \frac{1}{2}\int_A p v_a^* \, \mathrm{d}S. \tag{33}$$

Here, p and v_a are sound pressure and the particle velocity amplitudes, respectively, at a control surface S [17,32].

5.2. Effect of isolator material

The effect of isolator material properties is quantified in terms of insertion losses (IL). Sound pressure (p), vibration velocity (v) and acoustic power (Π_{RAD}) are calculated, where,

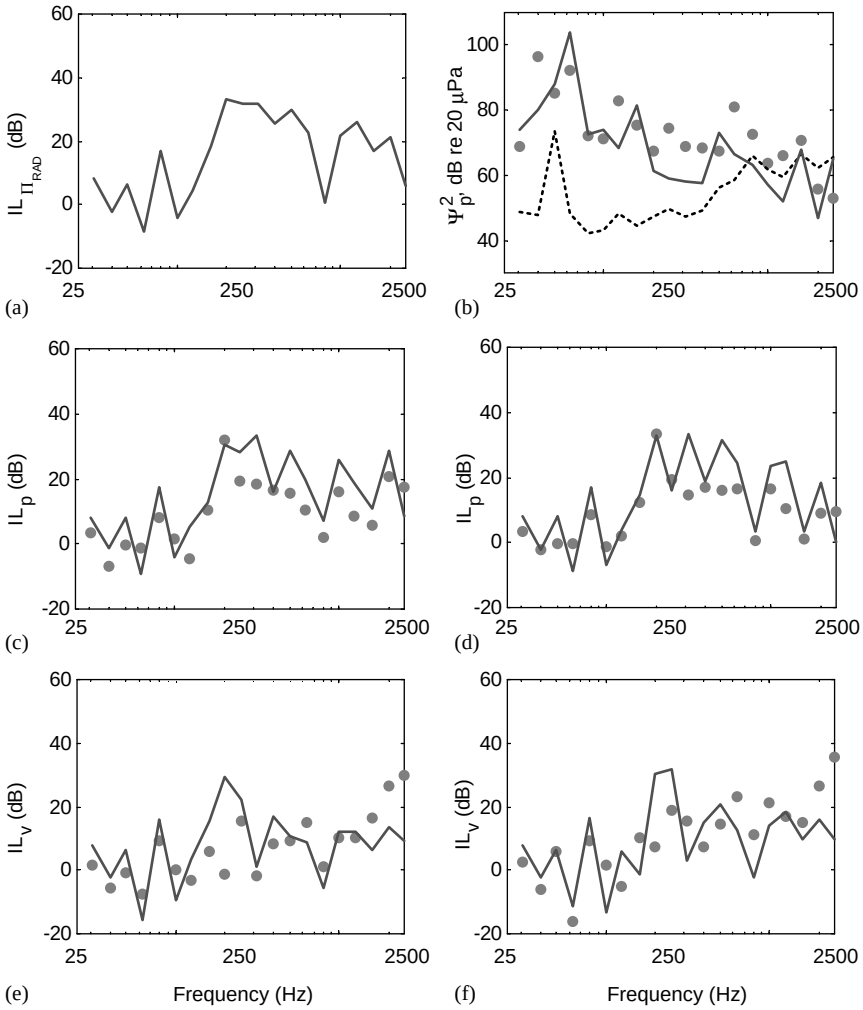

Fig. 17. Vibration isolation measures on mount material effect for isolator I given force excitation: (a) insertion loss ($IL_{\Pi_{RAD}}$) of acoustic power radiated from the 'L' plate receiver; (b) mean-square sound pressure (Ψ_p^2) at location ξ_1 of Table 4 with mount configuration of Fig. 14(a); (c) insertion loss (IL_p) of sound pressure at field location ξ_1; (d) IL_p at location ξ_2; (e) insertion loss (IL_v) of velocity at plate location ξ_3; (f) IL_v at location ξ_4. ——, calculated; •, measured; ……, background noise from shakers. Results are given in terms of 1/3 octave band center frequencies from 31.5 to 2500 Hz. Only the mean values within each bandwidth are plotted here.

in dB,

$$IL_{p_i} = 10\log_{10}\left(\frac{\Psi^2_{p_i,A}}{\Psi^2_{p_i,B}}\right), \quad IL_{v_j} = 10\log_{10}\left(\frac{\Psi^2_{v_j,A}}{\Psi^2_{v_j,B}}\right), \tag{34a, b}$$

$$IL_{\Pi_{RAD}} = 10\log_{10}\left(\frac{\Pi_{RAD,A}}{\Pi_{RAD,B}}\right). \tag{34c}$$

Here, p_i and v_j are sound pressure at acoustic field point i and velocity at receiver structure location j, respectively. Further, 'A' and 'B' represent the system with an aluminum and rubber (or polypropylene) isolator, respectively. The IL_p and IL_v spectra are obtained from both experimental and computational studies but only the computed results are used for $IL_{\Pi_{RAD}}$. The results are given at the center frequencies of the 1/3 octave band. Each isolator of Figs. 14(c) and (d) is separately examined and the mount location is unchanged for all cases. Experimental and computational results at the response locations (ξ) of Table 4 are shown in Figs. 17 and 18 for isolators I and II, respectively, when force (y) is applied at the mass center of a rigid body source. Further, the measured force inputs are used for computational studies. Resulting vibration and acoustic measures cannot be normalized with respect to their excitation forces since two different input forces are used. However, it is observed that measured input forces from the shaker stingers to a mass source do not vary much given different system configurations. Figs. 17 and 18 show that vibration and noise transmissions are much reduced over a wide range of frequencies when a rubber isolator with a lower G is used in place of an aluminum isolator. Further, $IL_{\Pi_{RAD}}$ spectra for sound power radiated from the 'L' plate receiver match well with the IL_p spectra for sound pressure, especially at location ξ_1. However, the experiment results of IL_p do not exhibit as much reduction as the ones computed beyond 500 Hz. One of the reasons is that the actual sound radiated from the receiver is lower than shaker noise beyond 500 Hz, especially when a rubber isolator is located at the center of source. See Figs. 17(b) and 18(b) where the background noise from shakers is also shown with mean-square sound pressure (Ψ_p^2). Note that the measured Ψ_p^2 of the system shows almost the same level as the Ψ_p^2 of shakers as shown in Figs. 17(b) and 18(b). Further, note that IL_v spectra, that are not contaminated by shaker noise, are much higher than IL_p beyond 500 Hz as shown in Figs. 17(c), (d) and 18(c), (d). Observe that the IL_v from experiments reasonably match with predicted IL_v as shown in Figs. 17(e), (f) and 18(e), (f). However, relatively large discrepancies between measured and predicted insertion losses are observed for isolator II of Fig. 18 at some frequencies, say 250–800 Hz. One reason for this may be the interfacial conditions of the isolators. For example, the polypropylene isolator (II) is connected through a plastic thread with the receiver plate and source mass, unlike the other three isolators. Also, refer to Fig. 14 for isolator shapes and material, and note that the rubber isolator I has aluminum interfacial plates at both ends of the isolator, unlike isolator II. Therefore, errors in the measurements of insertion loss, which compares the polypropylene and aluminum isolators (II), may be pronounced for isolator II. Yet, the elastomeric non-linearities could introduce other errors. For example, the polypropylene isolator (II) could have preload and amplitude dependencies and could exhibit spectrally varying material properties, unlike metallic mounts. Note that we have assumed spectrally invariant properties for the four isolator examples. Spectral averages of measured and computed results are shown in Table 6 for insertion losses. Overall, reasonable agreements between computed and experimental results are observed even though some measurements are contaminated by the shaker noise. Further, the root cause of the relatively larger discrepancies for some isolators (for example, the polypropylene isolator case), which may be due to interfacial conditions and/or elastomeric non-linearities, needs to be further studied.

5.3. *Effect of isolator location*

Next, the effects of mount location are examined using the experimental system of Fig. 14. Only the rotational free velocity of the source should exist for the moment excitation case when a

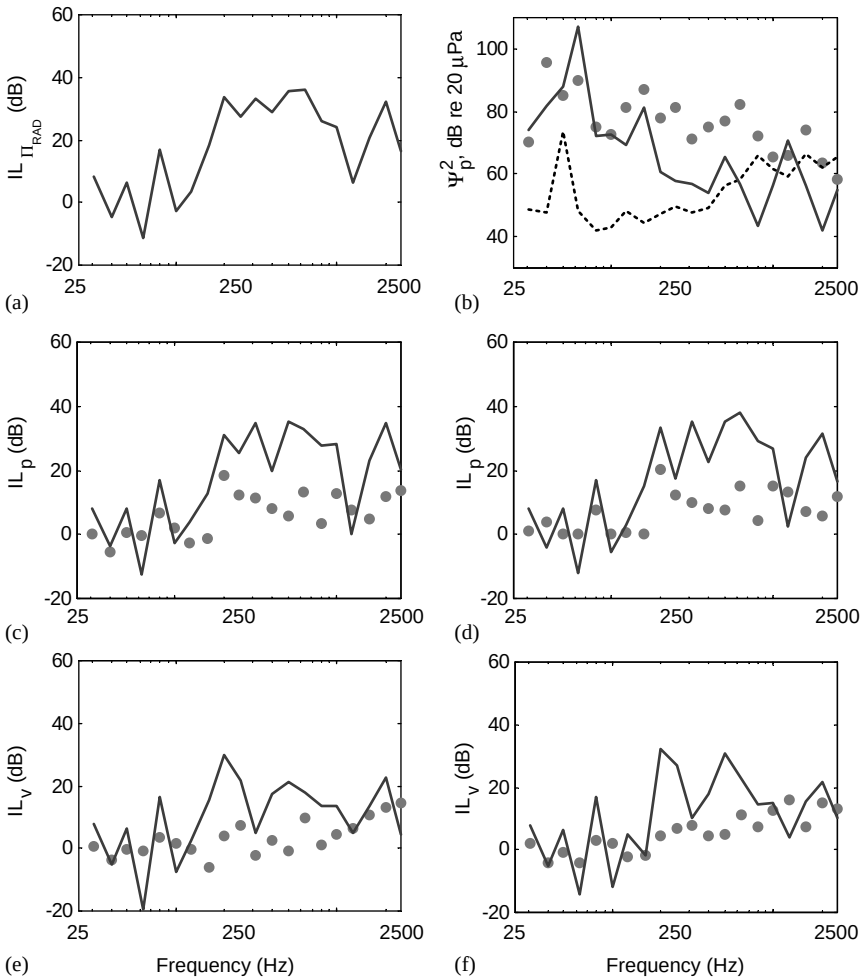

Fig. 18. Vibration isolation measures on mount material effect for isolator II given force excitation: (a) insertion loss ($IL_{\Pi_{RAD}}$) of acoustic power radiated from the 'L' plate receiver; (b) mean-square sound pressure (Ψ_p^2) at location ξ_1 of Table 4 with mount configuration of Fig. 13(a); (c) insertion loss (IL_p) of sound pressure at field location ξ_1; (d) IL_p at location ξ_2; (e) insertion loss (IL_v) of velocity at plate location ξ_3; (f) IL_v at location ξ_4. ——, calculated; •, measured; ……, background noise from shakers. Results are given in terms of 1/3 octave band center frequencies from 31.5 to 2500 Hz. Only the mean values within each bandwidth are plotted here.

mount is located at the center of the mass source. And, both translational and rotational free velocities occur when the isolator is placed at the edge of the rigid body source [12]. Similar to the previous cases, insertion losses (IL) are calculated by using Eqs. (34a)–(34c). In this case, subscript 'A' and 'B' refer to the cases when the isolator is placed at the edge and at the center of the mass respectively. First, consider the rubber and polypropylene isolator (I) cases of Figs. 19(a), (c) and 20(a), (c), where both computational and experimental results show that all vibration and sound measures are significantly reduced when an isolator is moved from the edge to the mass center. Like the previous case, measured IL_p spectra do not exhibit as much reduction as the ones computed beyond 500 Hz because the actual sound radiated from the receiver is lower than the

Table 6
Spectral averages of insertion losses for the experimental system of Fig. 13

Effect	Measure (mean-square value)	Isolator	Computation (dB)		Experiment (dB)	
			at ξ_1 or ξ_3	at ξ_2 or ξ_4	at ξ_1 or ξ_3	at ξ_2 or ξ_4
Isolator material given force excitation	Velocity (Ψ_v^2) at ξ_3 or ξ_4	Isolator I[a]	8	9	7	11
		Isolator II[b]	10	11	3	5
	Sound pressure (Ψ_p^2) at ξ_1 or ξ_2	Isolator I[a]	15	13	10	9
		Isolator II[b]	17	17	6	7
Isolator location given moment excitation	Velocity (Ψ_v^2) at ξ_3 or ξ_4	Rubber I[c]	22	22	20	18
		Aluminum I[c]	7	4	11	6
		Polypropylene II[c]	25	26	24	24
		Aluminum II[c]	9	5	11	12
	Sound pressure (Ψ_p^2) at ξ_1 or ξ_2	Rubber I[c]	21	22	15	15
		Aluminum I[c]	7	8	7	8
		Polypropylene II[c]	24	25	20	20
		Aluminum II[c]	7	9	10	11

[a] Baseline for insertion loss calculation is System with Rubber isolator I.
[b] Baseline for insertion loss calculation is System with Polypropylene isolator II.
[c] Baseline for insertion loss calculation is System with a mount located at the center of the mass source.

shaker noise beyond 500 Hz, especially when a rubber isolator is located at the center of the source. Further, similar to the previous case, IL_v spectra beyond 500 Hz are much higher than IL_p since measured IL_v are not contaminated by the shaker noise. Next, aluminum isolators (I and II) are examined. Figs. 19(b), (d) and 20(b), (d) show that vibration and acoustic measures are reduced by connecting an aluminum mount at a source location with zero translational free velocity. However, the aluminum isolator cases show less reduction when compared to the rubber or polypropylene isolator case. Further, it is observed in Figs. 19(b) and (d) that measured IL_p values exhibit a reasonable match with computed IL_p since the sound pressures with an aluminum mount are higher than the shaker noise level. Similar to the mount material case, spectral averages of the measured and computed insertion losses are again shown in Table 6. It is observed that significant reductions in vibration transmission, based on mount locations, are identified by using sound pressure measures for a system with Rubber I or Polypropylene II isolator. Velocity measures at selected locations also provide large reductions in vibration transmitted to a receiver, as seen from Table 6. Further, some reductions in velocity and sound measures are observed for a system with an aluminum isolator. Like the previous case, reasonable agreements between computed and experimental results are observed even though some measurements are contaminated by the shaker noise as discussed before.

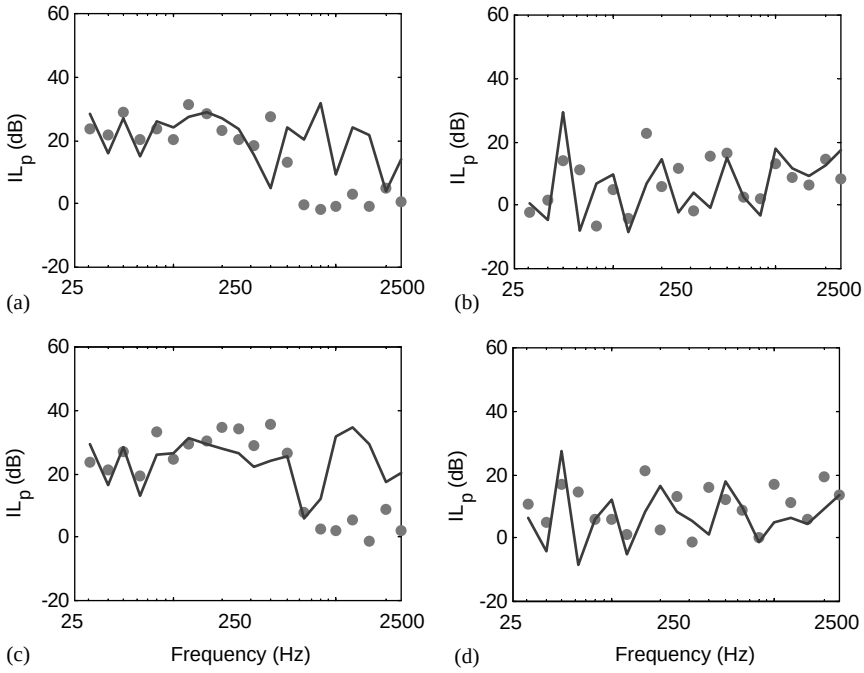

Fig. 19. Insertion loss (IL_p) of sound pressure at field location ξ_1 of Table 4 on mount location given moment excitation: (a) rubber isolator I; (b) aluminum isolator I; (c) polypropylene isolator II; (d) aluminum isolator II. ——, calculated; •, measured. Results are given in terms of 1/3 octave band center frequencies from 31.5 to 2500 Hz. Only the mean values within each bandwidth are plotted here.

6. Conclusion

6.1. Summary

Several measures of vibration isolation performance have been critically examined for a multi-dimensional system with inverted 'L' structure receivers. Non-dimensional components of multi-dimensional transmissibilities and effectivenesses are comparatively evaluated for an inverted 'L' beam receiver and four source configurations. Radiated sound pressures resulting from both in-plane and out-of plane motions of the 'L' beam receiver, have also been calculated and correlated with power-based measures. Further, vibration power components transmitted to the 'L' beam receiver and their interactions have been analyzed. Our analysis shows that significant couplings occur between different degrees of freedom. In order to efficiently interpret transfer paths of inherent complexity, several measures have been examined. Sound measurements and predictions for the inverted 'L' plate demonstrate that a rank order based on free field sound pressures, at one or more properly selected points, could be regarded as a measure of the vibration power transmitted to the receiver. Measured insertion losses for sound pressure match well with those based on computed results, especially on the basis of spectrally averaged values. Finally, the effects of interfacial conditions and elastomeric non-linearities need to be further studied.

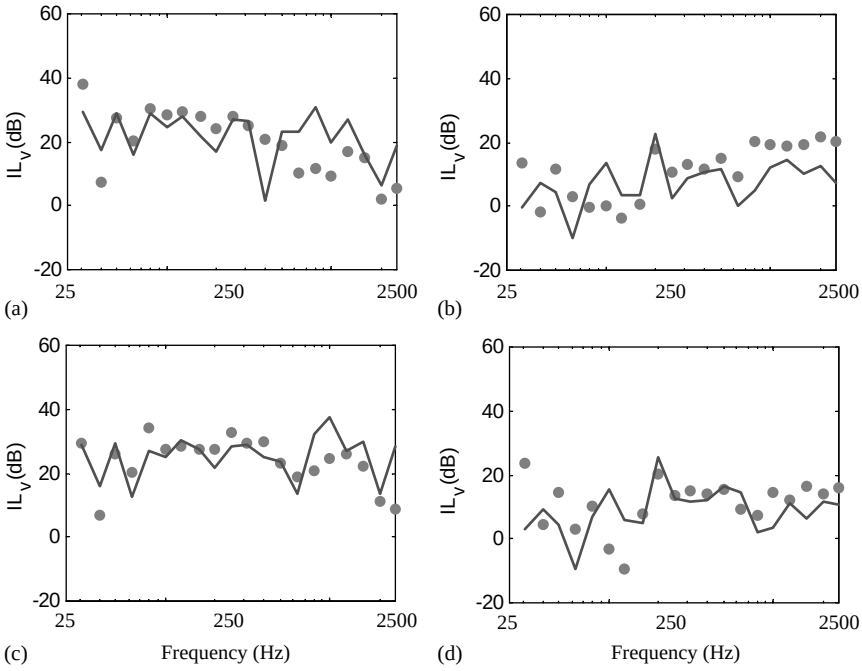

Fig. 20. Insertion loss (IL_v) of velocity at plate location ξ_3 of Table 4 on mount location given moment excitation. (a) Rubber isolator I; (b) aluminum isolator I; (c) polypropylene isolator II; (d) aluminum isolator II. ——, calculated; •, measured. Results are given in terms of 1/3 octave band center frequencies from 31.5 to 2500 Hz. Only the mean values within each bandwidth are plotted here.

6.2. *Emerging research issues*

Properties of elastomeric and hydraulic isolators typically show frequency dependency and are sensitive to preload and dynamic excitation levels [2,3]. In order to properly predict the isolation behavior of such non-linear systems, one must question the use of measures that are typically derived based on the linear system theory [35]. Several experimental methods have been developed to characterize the stiffnesses of an isolator. Direct force measures have been pursued by simulating ideal boundary conditions [36,37] but such approaches are limited to lower frequencies since the unwanted dynamics of the measurement machine is involved as the frequency increases [36]. Recently, some approximate methods that are based on motion transmissibilities have also been developed [38–41]. However, alternate laboratory measurement methods need to be correlated using appropriate isolation measures.

Simplified isolator models are often employed to describe the dynamic behavior of vibration isolation systems [3,5,11,15,16,42]. These are often longitudinal spring models [3,5,11] though some models include flexural components with or without the cross-axis coupling terms [15,16,42]. However, it is known that the rotational component becomes important and standing wave effects occur within an isolator as the frequency increases [1,4,42]. Therefore, more advanced isolator models are needed to properly describe couplings among multiple and/or multi-dimensional transmission paths [12,24–27]. Both driving and transfer point stiffnesses must be known to properly interpret isolator measures.

Several efforts have been made to quantify the contribution of source to vibration transmission to a receiver [12,23–27]. One may introduce a source descriptor along with an effective mobility concept to quantify the source contribution [23–27]. Further, the role of free source velocity on vibration transmission has been emphasized [12] and recently a "pseudo-force" method has been developed to simulate the free velocities of a source [43,44]. However, a more appropriate quantification of source strength is still required and dynamic interactions between sources and paths would need further investigation, especially in the presence of compliant vibration sources. Finally, future work is required to properly interpret coupling phenomena and to develop efficient transfer path measures for 'real life' systems that incorporate multiple isolators. Efforts are also needed to identify appropriate measures for structure-borne and airborne noise paths over a broad range of frequencies.

Acknowledgements

The General Motors Corporation (Noise and Vibration Center) and the Goodyear Tire and Rubber Company (Transportation Molded Products) are gratefully acknowledged for supporting this research.

Appendix A. Nomenclature

A, B, C, D	arbitrary constants
b	width
c	wave speed
d	distance to sound observation point from reference
E	Young's modulus
f	force amplitude
$\mathbf{f}$	force amplitude vector
F	excitation
$\mathbf{F}$	excitation vector
g	function for sound pressure
G	shear modulus
$\mathbf{G}$	function vector for sound pressure
h	reference location in rigid body with respect to mass center
I_S	area moment of inertia
I_m	mass moment of inertia
$\mathbf{I}$	identity matrix
IL	insertion loss
j	$\sqrt{-1}$
k	wave number
ℓ	length
m	mass
$\mathbf{m}$	inertia matrix

M	mobility
$\mathbf{M}$	mobility matrix
p	sound pressure
q	moment amplitude
$\mathbf{q}$	moment amplitude vector
Q	numerical constant for rubber material
$\mathbf{R}$	rotation matrix for the cross vector product
r	radius
S	area
S, P, R	source, path and receiver
t	thickness
$\mathbf{T}$	transformation matrix
T	shape factor
TR	transmissibility
$\mathbf{TR}$	transmissibility matrix
v	translational velocity
$\mathbf{v}$	translational velocity vector
V	velocity
$\mathbf{V}$	velocity vector
w	rotational velocity
$\mathbf{w}$	rotational velocity vector
X	displacement in x direction
Y	displacement in y direction
$\mathbf{X}$	generalized co-ordinate vector
x, y, z	cartesian co-ordinates
α, β, γ	mobilities of components
$\boldsymbol{\alpha}, \boldsymbol{\beta}, \boldsymbol{\gamma}$	mobility matrices of components
Γ	structural power efficiency
η	loss factor
θ	rotational displacement
ξ	response location
Ξ	effectiveness
$\boldsymbol{\Xi}$	effectiveness matrix
Π	vibration power (time-averaged)
ρ	mass density
Ψ	mean-square
ω	frequency, rad/s

Subscripts

a	air
A	axial (power)
B	flexural motion or bending (power)
G	mass center
H	horizontal beam or plate

IN	input
i, *j*	indices or reference points in mass
ℓ	lateral (power)
L	axial or longitudinal motion
p	perimeter
Q	variable
R	rotational
RAD	radiated
S, *P*, *R*	source, path and receiver
SAvg	spectral average
TR	transmitted out
V	vertical beam or plate
w	rotational component of mobility matrix of rigid body
W	weighted
WF	weighted force
WV	weighted velocity
with	with isolator
without	without isolator
x, *y*, *z*	cartesian co-ordinates
1, 2, 3, 4	reference locations

Superscripts

b	blocked
f	free
T	transpose
$\sim$	complex valued
.	time derivative
*	complex conjugate

Operators

diag	diagonal matrix
Re	real part
$\langle\ \rangle$	time-averaged
/	quotient for matrices

References

[1] L.L. Beranek, Noise and Vibration Control, Institute of Noise Control Engineering, Washington, DC, 1988.
[2] C.M. Harris, Shock and Vibration Handbook, McGraw-Hill, New York, 1987.
[3] J.C. Snowdon, Vibration and Shock in Damped Mechanical Systems, Wiley, New York, 1968.
[4] E.E. Ungar, C.W. Dietrich, High-frequency vibration isolation, Journal of Sound and Vibration 4 (2) (1966) 224–241.
[5] J.I. Soliman, M.G. Hallam, Vibration isolation between non-rigid machines and non-rigid foundations, Journal of Sound and Vibration 8 (2) (1968) 329–351.

[6] N.M.M. Maia, J.M.M. Silva, A.M.R. Ribeiro, The transmissibility concept in multi-degree-of-freedom systems, Mechanical Systems and Signal Processing 15 (1) (2001) 129–137.
[7] D.A. Swanson, L.R. Miiler, M.A. Norris, Multidimensional mount effectiveness for vibration isolation, Journal of Aircraft 31 (1) (1994) 188–196.
[8] A.O. Sykes, Development and Application of Linear Multi-terminal Network Theory to Vibration Problems, Ph.D. Thesis, The Catholic University of America, Washington, DC, USA, 1968.
[9] Y.K. Koh, R.G. White, Analysis and control of vibrational power transmission to machinery supporting structures subjected to a multi-excitation system, Part II: vibrational power analysis and control schemes, Journal of Sound and Vibration 196 (4) (1996) 495–508.
[10] H.G.D. Goyder, R.G. White, Vibrational power flow from machines into built-up structures, Part II: wave propagation and power flow in beam-stiffened plates, Journal of Sound and Vibration 68 (1) (1980) 77–96.
[11] H.G.D. Goyder, R.G. White, Vibrational power flow from machines into built-up structures, Part III: power flow through isolation systems, Journal of Sound and Vibration 68 (1) (1980) 97–117.
[12] S. Kim, Structure-borne Noise Transmission Through a Multi-dimensional Vibration Isolator, Ph.D. Thesis, The Ohio State University, Columbus, OH, 2001.
[13] R.J. Pinnington, Vibrational power transmission to a seating of a vibration isolated motor, Journal of Sound and Vibration 118 (3) (1987) 515–530.
[14] R.J. Pinnington, R.G. White, Power flow through machine isolators to resonant and non-resonant beams, Journal of Sound and Vibration 75 (2) (1981) 179–197.
[15] J. Pan, J. Pan, C.H. Hansen, Total power flow from a vibrating rigid body to a thin panel through multiple elastic mounts, Journal of the Acoustical Society of America 92 (2) (1992) 895–907.
[16] W.L. Li, P. Lavrich, Prediction of power flows through machine vibration isolators, Journal of Sound and Vibration 224 (4) (1999) 757–774.
[17] L. Cremer, M. Heckle, Structure-Borne Sound: Structural Vibrations and Sound Radiation at Audio Frequencies, Springer, New York, 1973.
[18] R.H. Lyon, R.G. Dejong, Theory and Application of Statistical Energy Analysis, Butterworth-Heinemann, Boston, 1995.
[19] T.E. Rook, R. Singh, Mobility analysis of structure-borne noise power flow through bearings in gearbox-like structures, Noise Control Engineering Journal 44 (2) (1996) 69–78.
[20] P. Gardonio, S.J. Elliott, R.J. Pinnington, Active isolation of structural vibration on a multiple-degree-of-freedom system, Part I: the dynamics of the system, Journal of Sound and Vibration 207 (1) (1997) 61–93.
[21] S. Kim, R. Singh, Vibration transmission through an isolator modelled by continuous system theory, Journal of Sound and Vibration 248 (5) (2001) 925–953.
[22] R.H. Lyon, Vibration transmission in machine structures, Noise Control Engineering Journal May-June (1993) 92–103.
[23] J.M. Mondot, B.A.T. Petersson, Characterization of structure-borne sound sources: the source descriptor and the coupling function, Journal of Sound and Vibration 114 (3) (1987) 507–518.
[24] R.A. Fulford, B.M. Gibbs, Structure-borne sound power and source characterisation in multi-point-connected systems, Part 1: case studies for assumed force distributions, Journal of Sound and Vibration 204 (4) (1997) 659–677.
[25] R.A. Fulford, B.M. Gibbs, Structure-borne sound power and source characterization in multi-point-connected systems, Part 2: about mobility functions and free velocities, Journal of Sound and Vibration 220 (2) (1999) 203–224.
[26] B.A.T. Petersson, Use of source descriptor concept in studies of multi-point and multi-directional vibrational sources, Journal of Sound and Vibration 160 (1) (1993) 43–66.
[27] B.A.T. Petersson, J. Plunt, On effective mobilities in the prediction of structure-borne sound transmission between a source and a receiving structure, Part 1: theoretical background and basic experimental studies, Journal of Sound and Vibration 82 (4) (1982) 517–529.
[28] T. ten Wolde, G.R. Gadefelt, Development of standard measurement methods for structure-borne sound emission, Noise Control Engineering Journal January-February (1987) 5–14.

[29] S. Kim, R. Singh, Multi-dimensional characterization of vibration isolators over a wide range of frequencies, Journal of Sound and Vibration 245 (5) (2000) 877–913.
[30] R.E.D. Bishop, D.C. Johnson, The Mechanics of Vibration, Cambridge University Press, Cambridge, 1960.
[31] L.E. Kinsler, A.R. Frey, A.B. Coppens, J.V. Sanders, Fundamentals of Acoustics, Wiley, New York, 1982.
[32] F. Fahy, Sound and Structural Vibration: Radiation, Transmission and Response, Academic Press, London, 1985.
[33] I-deas Users Manual Version 8.2. 2000 SDRC, USA.
[34] Sysnoise Users Manual Version 5.4. 1999 NIT, Belgium.
[35] T. Jeong, R. Singh, Inclusion of measured frequency- and amplitude-dependent mount properties in vehicle or machinery models, Journal of Sound and Vibration 245 (3) (2001) 385–415.
[36] MTS Systems Corporation, Test Star II Control System User Manual-Dynamic Characterization, 1999, p. 40.
[37] S. Nadeau, Y. Champoux, Application of the direct complex stiffness method to engine mounts, Experimental Techniques May/June (2000) 21–23.
[38] D.J. Thompson, N. Vincent, Track dynamic behavior of at high frequencies, Part 1: theoretical models and laboratory measurements, Vehicle System Dynamics Supplement 24 (1995) 86–99.
[39] D.J. Thompson, J.W. Verheij, The dynamic behavior of rail fasteners at high frequencies, Applied Acoustics 52 (1997) 1–17.
[40] D.J. Thompson, W.J. Van Vliet, J.W. Verheij, Development of the indirect method for measuring the high frequency dynamic stiffness of resilient isolator, Journal of Sound and Vibration 213 (1) (1998) 169–188.
[41] Å. Fenander, Frequency dependent stiffness and damping of railpads, Journal of Rail and Rapid Transit, Proceedings of Institute of Mechanical Engineers Part F 211 (1997) 51–62.
[42] M.A. Sanderson, Vibration isolation: moments and rotations included, Journal of Sound and Vibration 198 (2) (1996) 171–191.
[43] M.H.A. Janssens, J.W. Verheij, The use of an equivalent forces method for the experimental quantification of structural sound transmission in ships, Journal of Sound and Vibration 226 (2) (1999) 305–328.
[44] M.H.A. Janssens, J.W. Verheij, A pseudo-forces methodology to be used in characterization of structure-borne sound sources, Applied Acoustics 61 (2000) 285–308.